

**FLORIDA STATE UNIVERSITY**  
**FAMU-FSU COLLEGE OF ENGINEERING**

**THERMAL ANALYSIS OF A SOLAR WATER  
DISTILLATION AND ELECTRICITY  
GENERATION SYSTEM**

By

NIKHIL J. ANTHONY

A Thesis submitted to the  
Department of Mechanical Engineering  
in partial fulfillment of the  
requirements for the degree of  
Master of Science

Degree Awarded:  
Fall Semester, 2008

The members of the Committee approve the Thesis of Nikhil Anthony defended on August 27<sup>th</sup>, 2008.

---

Juan Carlos Ordonez  
Professor Directing Thesis

---

Farrukh S. Alvi  
Committee Member

---

William S. Oates  
Committee Member

Approved by:

---

Chiang Shih, Chair, Department of Mechanical Engineering

---

Ching-Jen Chen, Dean, FAMU-FSU College of Engineering

The Office of Graduate Studies has verified and approved the above named committee members.

## **ACKNOWLEDGEMENTS**

I would like to thank Dr. Juan Carlos Ordonez and Dr. Jose V.C. Vargas for their guidance and support in my work at the Center for Advanced Power Systems. I would like to thank my committee members for their advice and support.

I would like to thank my parents Mary and Anthony, my sister Reshma and brother Renil for their love and support.

I would like to thank my friends for their love and for helping me out with the experiments.

# TABLE OF CONTENTS

LIST OF FIGURES .....	v
LIST OF TABLES .....	vii
ABSTRACT .....	viii
1. INTRODUCTION .....	1
1.1 Literature review of current distillation systems .....	1
1.2 Motivation .....	5
2. THERMAL ANALYSIS OF THE SYSTEM .....	8
2.1 System modeling of photovoltaic cell .....	8
2.2 Thermal model for the photovoltaic cell .....	11
2.3 Thermal model for the cogeneration system .....	13
3. METHODOLOGY AND MATERIALS .....	21
3.1 Experiment to characterize I-V curves of Solara SM 200 S .....	21
3.2 Experiment to verify the thermal model of the photovoltaic system .....	26
4. RESULTS AND DISCUSSION .....	28
4.1 Photovoltaic cell performance .....	28
4.2 Thermal model of photovoltaic cell .....	33
4.3 Thermal model of cogeneration system .....	35
5. CONCLUSIONS AND SUGGESTIONS .....	49
REFERENCES .....	53
BIOGRAPHICAL SKETCH .....	55

## LIST OF FIGURES

Figure 1.1: Schematic diagram of a solar MED system [15].....	2
Figure 1.2: Principle of MSF (Multi-Stage Flash) [14].....	3
Figure 1.3: Configurations of membrane distillation modules: (a) direct-contact membrane distillation; (b) air-gap membrane distillation. ....	4
Figure 1.4: Schematic of still solar. ....	6
Figure 1.5: Solar Distiller used for removal of Arsenic from water by distillation.....	7
Figure 2.1: Circuit diagram of the photovoltaic cell including currents and resistances....	8
Figure 2.2: Schematic of the cogeneration system. ....	13
Figure 2.3: Control volume 4 (roof of cogeneration system). ....	17
Figure 3.1: Schematic of I-V characteristic measurements. ....	22
Figure 3.2: Arrangement of the pyranometer. ....	23
Figure 3.3: Arrangement to measure the current voltage characteristics of photovoltaic cell.....	24
Figure 3.4: Measurement of unsteady state Temperature of PV cell.....	26
Figure 3.5: Back of photovoltaic cell with thermocouples stuck with high thermally conducting paste.....	27
Figure 4.1: Comparison of calculated and experimental values of I-V characteristics for 300K module temperature and irradiance of 975 W/m <sup>2</sup> . ....	29
Figure 4.2: Comparison of calculated and experimental values of I-V characteristics for 323K module temperature and irradiance of 1000 W/m <sup>2</sup> . ....	30
Figure 4.3: Comparison of calculated and experimental values of I-V characteristics for 289K module temperature and irradiance of 525 W/m <sup>2</sup> . ....	31
Figure 4.4: Comparison of calculated and experimental values of I-V characteristics for 312K module temperature and irradiance of 962.5 W/m <sup>2</sup> . ....	32
Figure 4.5: Variation of the temperature of photovoltaic module with respect to temperature for a given constant irradiation (1000 W/m <sup>2</sup> ). ....	33

Figure 4.6: Irradiation varying in a sinusoidal manner with respect to time. ....	34
Figure 4.7: Plot of temperature of module with varying irradiance. ....	35
Figure 4.8: Variation of mass of vapor ( $m_v$ ) with time. ....	39
Figure 4.9: Variation of mass of water in CV4 with time. ....	40
Figure 4.10: Temperature variation of different control volumes with time. ....	41
Figure 4.11: Graph of temperature vs. time for different values of global heat transfer coefficient ( $U_{12}$ ). ....	43
Figure 4.12: Temperature variation of different control volumes with time ( $U_{12}=100$ W/m <sup>2</sup> K). ....	44
Figure 4.13: Variation of mass of vapor with time ( $U_{12} = 100$ W/m <sup>2</sup> K). ....	45
Figure 4.14: Current-Voltage characteristics of photovoltaic cell independently and when coupled with the cogeneration system. ....	46
Figure 4.15: Power produced by photovoltaic cell independently and when coupled with cogeneration system. ....	46
Figure 4.16: Temperature of control volumes under varying irradiance. ....	47
Figure 4.17: Variation of mass of vapor in vapor space (CV3) with time under a varying irradiance. ....	48
Figure 5.1: Variation of temperature of different control volumes. ....	49
Figure 5.2: Comparison of the power obtained by photovoltaic module. ....	50
Figure 5.3: Variation of mass of water produced with respect to time. ....	51

## LIST OF TABLES

Table 2.1: Mass diffusivity of air-water vapor gaseous mixture. ....	15
Table 4.1: Values of some parameters and constants considered during the simulation..	37

## **ABSTRACT**

Solar stills are a popular choice for distilling water and removing harmful contaminants like arsenic and other minerals in some rural parts of Argentina. The processes involved in solar still are environment friendly as they are driven only by solar energy and do not require any external energy sources (such as electricity or energy from combustible products). The objective of the current study is to couple such a solar still with a photovoltaic array in order to generate both potable water and electricity simultaneously. A model for such a system is developed and used to simulate the conditions of both constant and variable irradiation. It is found that the water which evaporates in the solar still extracts the heat from the photovoltaic module consequently decreasing its temperature. The photovoltaic array coupled with the cogeneration system operates at temperatures which are lower than a stand-alone cell, thereby increasing the efficiency of the cell. With water and electricity as the byproducts of the system, the efficiency of the entire system is increased. Details pertaining to thermal analysis of the system are discussed.

# CHAPTER 1

## INTRODUCTION

### 1.1 Literature review of current distillation systems

Filtration has been studied for quite some time now. It is defined as a method to separate solid particles from fluids by interposing a medium which will allow the fluid to pass through and trap the solid particles suspended in it; it is done mainly to purify fluids. This process is however ineffective for the impurities which are dissolved in the fluid. Sea water is a simple example of such a fluid, in which salt is dissolved. There are many places where potable water is a commodity, since the water available in such places has many dissolved impurities which make it unfit for drinking. Desalination is a process in which salt and other dissolved minerals are extracted from water. There are several technologies which are utilized for solar desalination. Some of the desalination techniques are discussed below.

Solar multi-effect distillation (MED) is generally used in large scale desalination. There are several stages in the MED system, the vapor from one stage of the system condenses in a second stage, where the heat of condensation is utilized to heat and evaporate the fluid in the second stage. A pressure which is lower than atmospheric pressure is maintained in the second stage, due to which water evaporates at a lower temperature in the second stage. This is repeated for several stages as shown in Figure 1.1. Except for the losses in the system in form of leakages, all the energy is utilized to evaporate the water at different stages. One of such multiple stage distillers is shown in the figure below. This system was studied as a potential desalination system as a viable alternate source in Jordan [15].

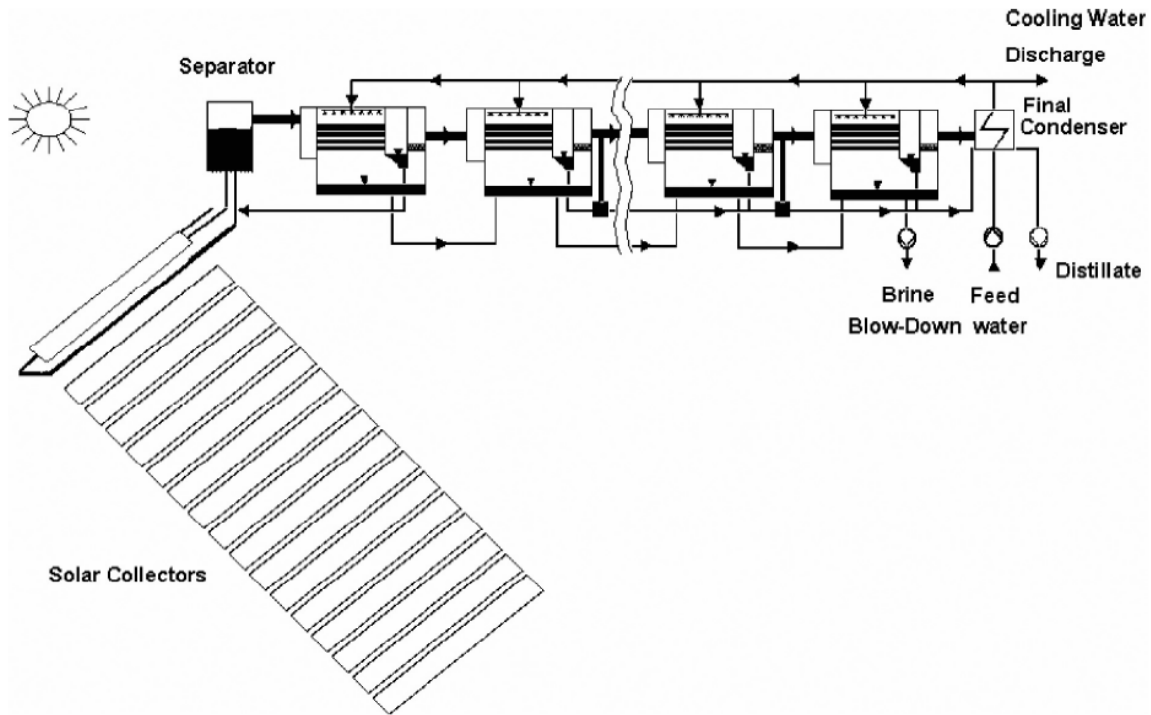


Figure 1.1: Schematic diagram of a solar MED system [15]

More water is produced as the number of stages increases but the investment to have different pressures and temperatures in different effects is increased. Since the pressure in the every stage is different, and lower than atmospheric, a system which maintains vacuum pressure in these stages is required. This adds up to the infrastructure and the power needs to run these systems also arises. MED is an effective system for desalination but, the investment is significant and also it is difficult to maintain.

Multistage flash (MSF) distillation is another method introduced in the 1960's to desalinate water [14]. It is reliable and simple; it uses the principle of evaporating water at progressively reduced pressure. 85% of the world's desalinated water is produced by this method [18]. The first step of MSF is to preheat the brine solution in a brine heating stage. This is achieved by passing the solution through tubes, the outer side of which is used for condensing steam. The preheated brine water can be heated to a higher temperature using external sources of energy (e.g. solar energy). The heated solution is introduced in a chamber which has a pressure lower than atmospheric. Due to the lower pressure, the water starts boiling and flashes into steam. A portion of the water is converted to steam; the remaining water is carried onto the next stage, where the pressure

is lower than the previous stage, boiling some portion of the remaining water. Thus the water is carried through a series of stages where water is converted to steam. The steam is condensed on the tubes above, passing the heat of condensation to the brine water. The condensed water, which is the desired product, is collected in trays. Figure 1.2 shows the principle of MSF.

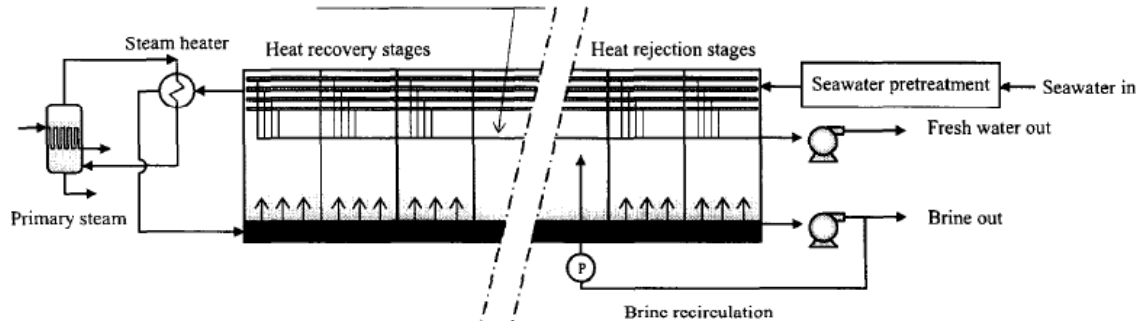


Figure 1.2: Principle of MSF (Multi-Stage Flash) [14].

This is an effective method around the world for the desalination of water with reliability and low operation costs. Since the temperature of the water coming in is low, there is a large amount of energy required to heat the water, these systems are thus utilized where the energy costs are low or where they can be coupled with power plants or cogeneration plants, where the water is heated primarily with the help of heat recovery systems.

Reverse osmosis is another effective method of producing water through desalination. In this process, saline water is forced through a semi-permeable membrane under pressure such that the, solvent is allowed to pass through the membrane while the solute is filtered. The water, under pressure is forced through the membrane while the membrane retains the solvent. This is an effective way to produce pure water; it is inexpensive and simple in operation compared to the other methods, although the pumping costs to pressurize water is significant. One disadvantage of such a system is that, the suspended particles in the water will clog the membrane, and the membrane can be damaged due to some chemical compounds present in the solution, this requires the water to be treated before reverse osmosis can be carried out. Reverse osmosis is an effective and inexpensive method of purifying water compared to the MSF and MED, but the pumping costs are still considerable [14].

Another inexpensive method of solar distillation is shown in [16] which couples the concept of solar stills with membrane distillation. Membrane distillation can best be described as trans-membrane evaporation. It is a thermally driven process in which a hydrophobic membrane is in contact with a hot or warm feed solution. Vapor evolved from the feed solution passes through the pores of the membrane and is collected on the other side. Methods for collecting the vapor permeate include immediate condensation within a colder liquid flowing on the second side of the membrane, Figure 1.3(a), or condensation on a cold surface located at some distance from the membrane, Figure 1.3(b) [16]. In the latter situation, vacuum can be applied to draw more vapors through the membrane. The Figure 1.3 shows the hybrid system.

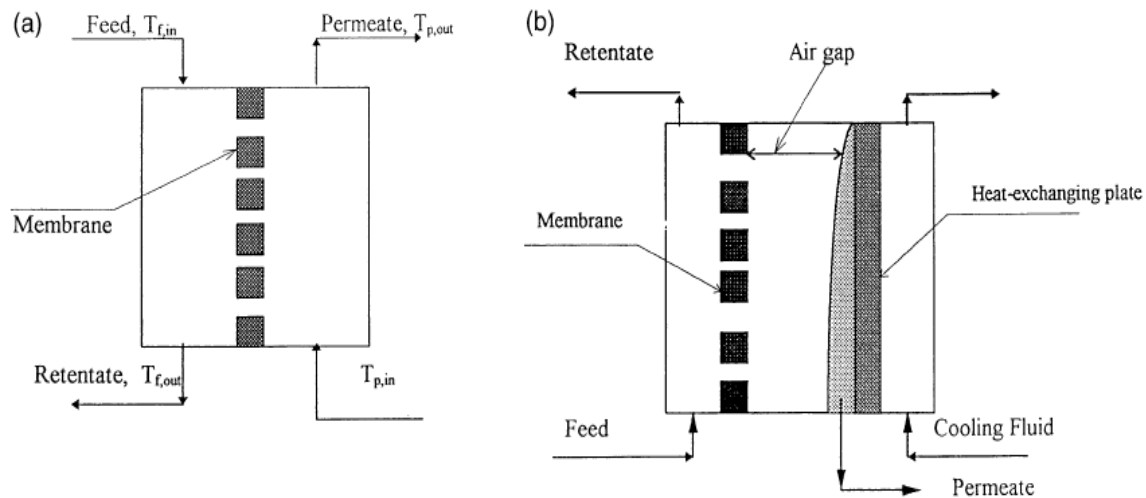


Figure 1.3: Configurations of membrane distillation modules: (a) direct-contact membrane distillation; (b) air-gap membrane distillation [16].

The major cost of such a system arises from the hydrophobic membrane and the infrastructure to have cooling systems for the cooling of the vapor on the other side of the membrane. Yet this seems to be an effective and inexpensive method of producing potable water in remote areas.

## 1.2 Motivation

As explained in the Introduction, there are several ways to desalinate water. The methods described are used for desalination based upon requirements and prevailing conditions. The objective of this work is to develop modeling tools that would help on the evaluation of the feasibility of combining solar desalination (using solar stills) and photovoltaic electricity generation. The aim is to develop a model of a simple, cost effective desalination system which can be applied on a small individual basis in remote areas where there is lack of infrastructure to produce distilled water by other means and in the process also produce electricity which is an important commodity in such areas. Large scale desalination plants require large amounts of energy and expensive infrastructure. The system which is under consideration utilizes solar energy to desalinate water and in the process also produces electricity through photovoltaic effect. This increases the efficiency of the system. Using solar irradiation for desalination is a cost effective method for producing water in remote areas where there are difficulties in supplying fossil fuels and there is no grid for any external power source. Production of electricity in such areas is also of great utility as the cost of installing grids or producing electricity through fossil fuels requires large infrastructure and is expensive to operate and maintain. The system studied in this report is self-sufficient. The operation and maintenance of such a system is simple and does not require any professional services.

The method of desalination used in this study is based on the principle of a solar still. A solar still is combined with a photovoltaic cell, thus producing distilled water and electricity from solar radiation. The solar still mimics the process of making of rain in nature. A simple solar still is shown in the Figure 1.4.

The saline water in the trough is heated up by the solar irradiation which is incident on it. This evaporates the water which increases the vapor pressure in the enclosure. The partial pressure of the vapor inside the enclosure goes on increasing to an extent where the relative humidity of vapor space reaches 100%, at which instant water starts condensing on the roof surface.

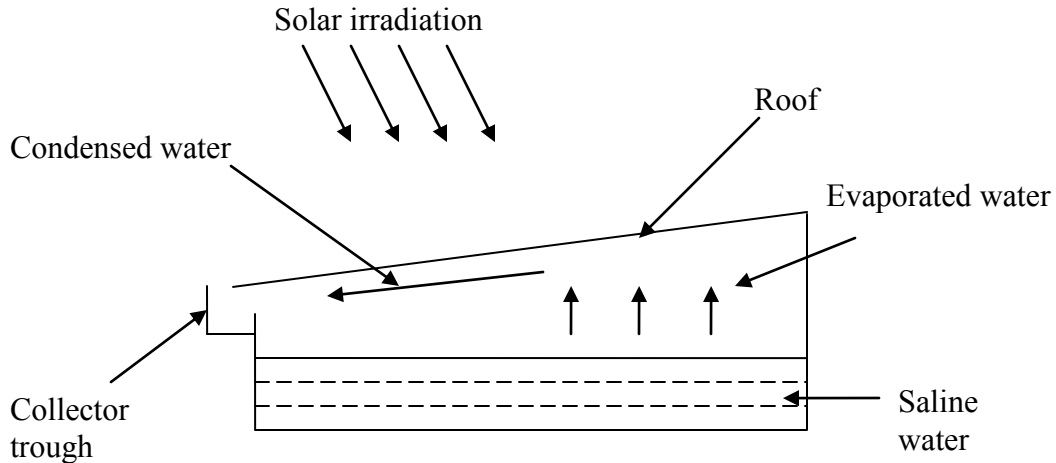


Figure 1.4: Schematic of still solar.

Water condensed on the roof trickles down the surface due to the inherent slope of the surface. This water is collected in the troughs as the end product of distillation. This is the principle of the solar still. As described above this process does not require any moving parts or any kinds of membranes for its operation.

The motivation for such a cogeneration model was inspired by the process carried out in parts of Argentina where this distillation process is incorporated to make the water free of Arsenic. Figure 1.5 shows the enclosure for such an arrangement.

The entire enclosure is to be made transparent to light and a photovoltaic array is coupled at the bottom of the reservoir such that it is in contact with water. The solar irradiation passes through the water in the enclosure heats it up and finally is incident on the photovoltaic cell. The solar irradiance incident on the photovoltaic cell is converted to electricity due to the inherent behavior of the photovoltaic cell. As explained in the following chapters, the efficiency of the photovoltaic cell depends on the temperature of the cell such that a higher temperature of the module will produce lower efficiency of the cell. In the system which is studied the water in the distiller will extract heat from the photovoltaic module in the process cooling it down.



Figure 1.5: Solar Distiller used for removal of Arsenic from water by distillation.

This results in the temperature of the solar module to be lower than when it is operating alone. This lower temperature corresponds to an increase in the efficiency of the photovoltaic module. The system described in this report thus produces a viable solution to produce fresh water and in the process increases the efficiency of the photovoltaic cell coupled to the system. The following chapters will discuss how such system is thermally modeled and solved numerically. Results and ways to enhance the system are also discussed.

## CHAPTER 2

### THERMAL ANALYSIS OF THE SYSTEM

#### 2.1 System modeling of photovoltaic cell

A photovoltaic cell behaves like a diode, with a *p-n junction*, space charge region and the neutral region. Due to the physics of the interaction of the electrons and holes at the *p-n junction*, there is a junction current ( $I_D$ ) also termed as diode current generated which depends on the temperature of the cell. This behavior of the cell in the absence of illumination is typical to the behavior of a diode, hence is modeled very similar to it. The diode current is a sum of the recombination current and dark current which is expressed as  $I_D = I_r - I_s$ . The dark current ( $I_s$ ) is the current flowing when the photovoltaic cell is in a dark condition. This is due to the thermal excitation of the electrons. The recombination current ( $I_r$ ) is present due to the some electrons having enough energy to cross the *p-n junction* in the opposite direction. The recombination current is proportional to dark current and given by

$$I_r = I_s e^{\left(\frac{e_0 V}{mkT}\right)} \quad (2-1)$$

$$\text{Therefore, } I_D = I_s \left( e^{\left(\frac{e_0 V}{mkT}\right)} - 1 \right) \quad (2-2)$$

The photovoltaic cell under illumination gives good results when modeled with the two diode model [7], as shown in Figure 2.1.

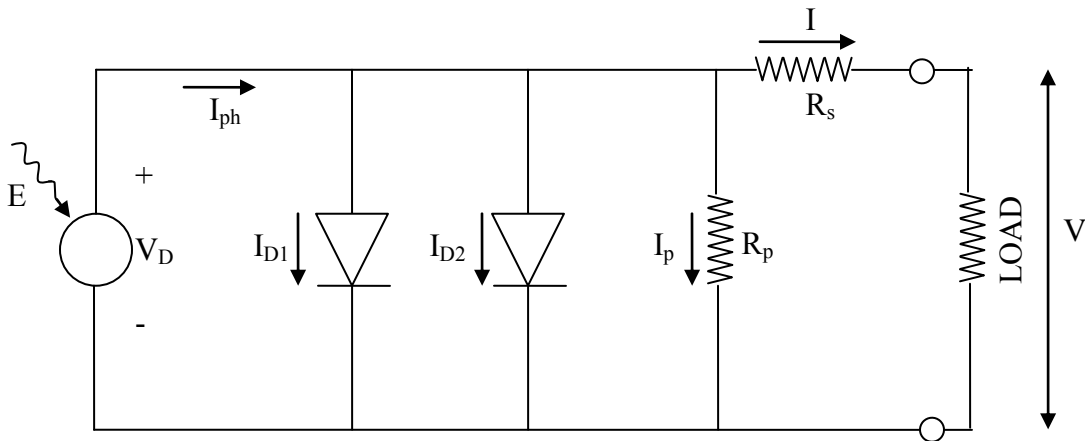


Figure 2.1: Circuit diagram of the photovoltaic cell including currents and resistances.

For the two diode model,

$$I = I_{ph} - I_{D1} - I_{D2} \quad (2-3)$$

Where  $I_{D1}$  is the diode current resulting from the current in the neutral region and  $I_{D2}$  is the diode current in the space charge region.

As the electrons pass over the *p-n junction*, there is some drop in the voltage, this drop in the voltage is accounted by having an internal resistance ( $R_s$ ) in series. There is some leakage at the edges of the cell which is modeled as a shunt resistor ( $R_p$ ) as shown in the Figure 2.1. The current  $I_p$  is modeled as  $V_D/R_p$ . The resulting double exponential equation which explains the I-V behavior of a photovoltaic cell is given below [7].

$$I = I_{ph} - I_{s1} \left( e^{\frac{e_0V}{m_1kT}} - 1 \right) - I_{s2} \left( e^{\frac{e_0V}{m_2kT}} - 1 \right) - \frac{(V + IR_s)}{R_p} \quad (2-4)$$

Where,

$I_{ph}$  – Photocurrent under illumination.

$I_{s1}$  – Reverse saturation current in neutral region.

$I_{s2}$  – Reverse saturation current in the space charge region.

$R_s$  – Series resistance to account for the voltage drop across the junction.

$R_p$  – Shunt resistance modeled for the leakage current.

$m_1$  – Diode parameter for neutral region ( $m_1=1$ )

$m_2$  – Diode parameter for neutral region ( $m_2=2$ )

$V$  – Voltage of a single Photovoltaic.

$e_0$  – Charge of electron.

$k$  – Boltzmann's Constant.

$T$  – Absolute temperature.

$I$  – Current obtained at load of single Photovoltaic cell.

There are five parameters  $\theta = [I_{ph}, I_{s1}, I_{s2}, R_s, R_p]$  which are unknown in equation (2-4). Experiments to characterize the I-V curve of a photovoltaic cell are carried out and the result is curve fitted into the double exponential equation using Levenberg-Marquardt method to find these parameters [11]. These parameters are not constant but change with the temperature (T) and irradiance (E). The relation for these parameters with respect to

temperature (T) and irradiance (E) for a cell satisfying the double exponential equation is taken from [11] and is given below

$$I_{ph} = K_0 E (1 + K_1 T) \quad (2-5)$$

$$I_{s1} = K_2 T^3 e^{\left(\frac{K_3}{T}\right)} \quad (2-6)$$

$$I_{s2} = K_4 T^{\left(\frac{3}{2}\right)} e^{\left(\frac{K_5}{T}\right)} \quad (2-7)$$

$$R_s = K_6 + \frac{K_7}{E} + K_8 T \quad (2-8)$$

$$R_p = K_9 e^{(K_{10} T)} \quad (2-9)$$

By substituting the 11 constants, the five parameters of the double exponential equation (2-4) can be solved for any value of temperature (T) and irradiance (E), the I-V characteristics and thus the power can be predicted for such condition.

Thus,

$$\begin{aligned} \theta &= [I_{ph}, I_{s1}, I_{s2}, R_s, R_p] \\ I &= I(V, \theta) \\ I &= I_{ph} - I_{s1} \left( e^{\left(\frac{e_0 V}{m_1 k T}\right)} - 1 \right) - I_{s2} \left( e^{\left(\frac{e_0 V}{m_2 k T}\right)} - 1 \right) - \frac{(V + I R_s)}{R_p} \\ \theta &= \theta(T, E) \\ I &= I(V, T, E) \end{aligned} \quad (2-10)$$

The power is given by

$$P = VI(V, T, E) \quad (2-11)$$

The current and voltage obtained is for a single cell, if higher voltage is desired, the cells are connected in series in a module which gives the total voltage as  $V_{total} = n \cdot V_{cell}$ . A higher current is obtained by placing cells in parallel in a module giving  $I_{total} = n \cdot I_{cell}$ . The desired current or voltage can be achieved by arranging the cells in combination of series and parallel.

## 2.2 Thermal model for the photovoltaic cell

A thermal model of the photovoltaic cell was made based upon the energy balance equations. Some of the energy which is incident on the module in form of irradiation is utilized to raise the temperature of the module, some of it is distributed in the form of losses to the surroundings in form of convection, radiation and the remaining is converted to power by photovoltaic effect of the module. An energy balance equation of this is written below.

$$\left[ \alpha_{PV} \dot{I} - \varepsilon_{PV} \sigma (T_1^4 - T_\infty^4) \right] A_{12} - U_{1\infty} A_{1\infty} (T_1 - T_\infty) - P = m_{PV} c_{PV} \frac{dT_1}{dt} \quad (2-12)$$

Where,

$\alpha_{PV} = 0.855$  [13], absorptivity of photovoltaic module.

$\dot{I}$  - Irradiation incident on the photovoltaic module.

$\varepsilon_{PV} = 0.85$  [13], emissivity of the photovoltaic module.

$\sigma = 5.6696 \times 10^{-8}$  (W/m<sup>2</sup>K<sup>4</sup>) Stephan Boltzmann constant.

$T_1$  – temperature of the module.

$T_\infty$  - Ambient temperature.

$A_{12}$  – Area of the module.

$U_{12}$ - Global heat transfer coefficient.

$m_{PV}$  – mass of photovoltaic module.

$c_{PV}$  – specific heat of the photovoltaic module.

$P$  – Power extracted from the photovoltaic cell.

$\alpha_{PV} \dot{I}$  is the energy absorbed by the module where  $\dot{I}$  is the energy incident on the photovoltaic module and  $\alpha_{PV}$  is the absorptivity of the module, the model was first tested at constant irradiation to find the module reached the steady state condition in time, then this model was verified for changing irradiation.

$\varepsilon_{PV} \sigma (T_1^4 - T_\infty^4)$  is the energy lost to the surroundings in form of radiation where  $\varepsilon_{PV}$  is the emissivity of the module and  $T_\infty$  is the temperature of the surroundings.

$U_{1\infty}A_{1\infty}(T_1 - T_\infty)$  is the energy lost to the surroundings by advection, where  $U_{1\infty}$  is the lumped global heat transfer coefficient which need to be verified by experimental validation.

$P$  is the power which is generated by the PV cell, when it is operation; this power is calculated by equation (2-11). The power calculated during simulation is the peak power at a given temperature.

$m_{PV}c_{PV} \frac{dT_1}{dt}$  represents the increase in the module's energy.

For the above differential equation (2-12), the initial condition is set as  $T_1 = T_\infty$  and is solved by Runge-Kutta method.

## 2.3 Thermal model for the cogeneration system

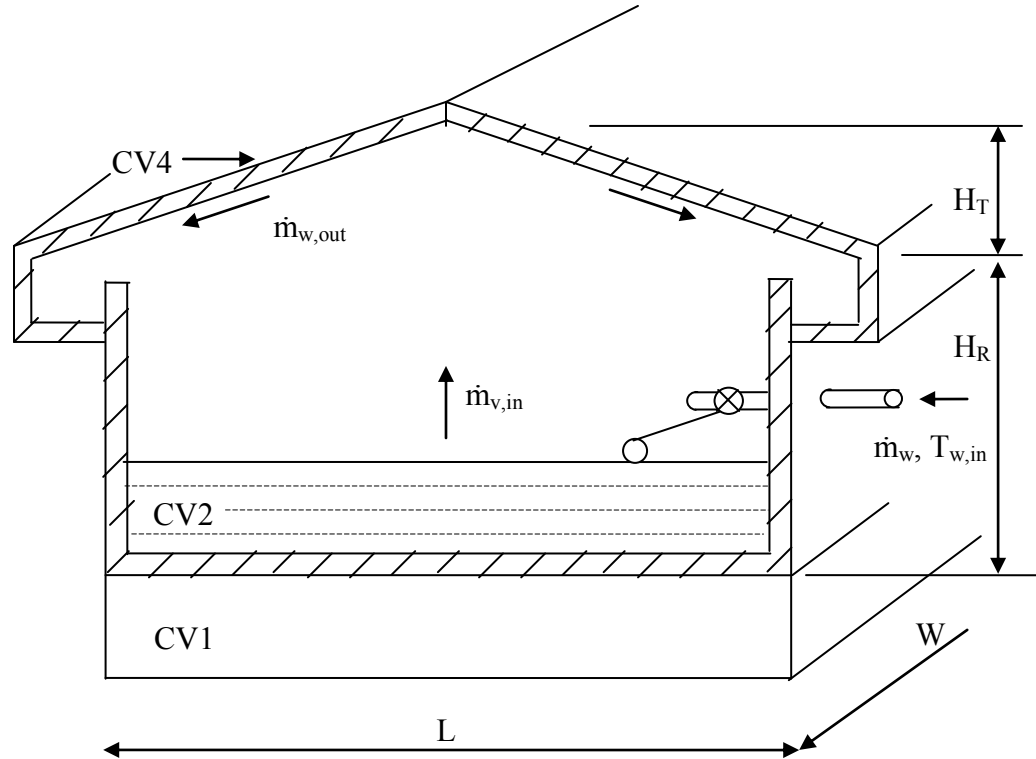


Figure 2.2: Schematic of the cogeneration system.  
 $L = 1\text{m}$ ,  $W = 2\text{m}$ ,  $H_T = 0.1\text{m}$ ,  $H_R = 0.07\text{m}$

A Control Volume analysis is used to analyze the given problem. Figure 2.2 shows the system which is divided into four Control Volumes (CV). Control Volume 1 (CV1) is the photovoltaic cell which is analyzed using the energy balance equation. Control Volume 2 (CV2) is the volume of water which is heated up in solar still. Control Volume 3 (CV3) is the space volume in which vapor is formed by the solar heating of the water in CV2. Control volume 4 (CV4) is the roof of the solar still on which vapor from CV3 condenses. CV2, CV3 and CV4 are analyzed by mass and energy balance equations as shown below.

### 2.3.1 Mass and energy analysis of CV3 (vapor space):

The model starts by writing the mass conservation statement for the water vapor in CV-3 as follows:

$$\frac{dm_v}{dt} = \dot{m}_{v,in} - \dot{m}_{v,out} \quad (2-13)$$

Mass transfer from water in CV2 to CV3:

$$\dot{m}_{v,in} = [\bar{h}_m A_{23}(\rho_w - \rho)] \quad (2-14)$$

where,

$\rho_w = \frac{1}{v_g(T_2)}$ , density of saturated vapor at temperature  $T_2$ , from a water saturation table.

$A_{23}$  – interface between CV2 and CV3, i.e., water surface area between CV2 and CV3.

$$\rho = M_{H_2O} \frac{\rho_a(T_3)}{M_a} x_v \quad (2-15)$$

$\rho_a$  – dry air density at temperature  $T_3$

$M_{H_2O}$  and  $M_a$  - Molecular weights of water and air respectively

$x_v$  – molar fraction of vapor in CV3

$$m_a = \rho_a(T_3)V_3 \quad (2-16)$$

$V_3$ - CV3 volume = constant

$$x_v = \frac{\frac{m_v}{M_{H_2O}}}{\frac{m_v}{M_{H_2O}} + \frac{m_a}{M_a}} \quad (2-17)$$

The partial pressure of vapor in CV3 is given by

$$p_v = p x_v \quad (2-18)$$

Where,  $p$  is the total pressure in CV3, i.e., which is atmospheric pressure.

The relative humidity in CV3 is calculated as follows:

$$\phi = \frac{p_v}{p_{v,sat}(T_3)} \quad (2-19)$$

When  $\phi=1$ , condensation starts on the inner surface of the roof and  $\dot{m}_{v,out} = \dot{m}_{v,in}$ , i.e.,

the clean water production starts, before that instant,  $\dot{m}_{v,out} = 0$

The average water vapor mass transfer coefficient is calculated based on the wetted

length,  $L_w = \frac{L+W}{2}$ , taken as the arithmetic mean of the length and width of the fluid

reservoir for a flat surface, considering there is an air velocity in CV3 due to natural convection (Bejan, 2004), as follows:

$$\overline{\text{Sh}}_{L_w} = 0.664 \text{Sc}^{\frac{1}{3}} \text{Re}_{L_w}^{\frac{1}{2}} \quad (2-20)$$

$$\overline{h}_m = \frac{D}{L_w} \overline{\text{Sh}}_{L_w} \quad (2-21)$$

$$\text{Re}_{L_w} = \frac{u_a L_w}{\nu_a} \quad (2-22)$$

Where,

Sc = 0.6 for water vapor in air, and

D = mass diffusivity of air-water vapor gaseous mixture at T<sub>3</sub>

Table 2.1: Mass diffusivity of air-water vapor gaseous mixture.

D (m <sup>2</sup> /s)	T <sub>3</sub> (K)
2.6e-5	298
2.88e-5	313

$$u_a \cong \alpha \left[ \frac{g\beta}{\alpha\nu_a} |T_3 - T_2| H \right]^{\frac{1}{2}} \quad (2-23)$$

This is velocity of air based on the flow due to natural convection.

Where,

$$\frac{g\beta}{\alpha\nu_a} = 90.7 \text{e}6 \text{ m}^{-3} \text{K}^{-1} \text{ for dry air @ } 30^\circ\text{C},$$

$$\alpha = 0.223 \text{e} - 4 \frac{\text{m}^2}{\text{s}} \text{ for dry air @ } 30^\circ\text{C},$$

$$\nu_a = 0.16 \text{e} - 4 \frac{\text{m}^2}{\text{s}} \text{ for dry air @ } 30^\circ\text{C},$$

$$H = H_T + H_R,$$

Therefore, Equation (2-13) delivers the water vapor mass at any given time, provided that an initial water vapor mass is given as an initial condition, from a know initial relative humidity,  $\phi_0$  as follows:

$$p_{v,0} = \phi_0 p_{v,sat}(T_{3,0}) \quad (2-24)$$

$$x_{v,0} = \frac{p_{v,0}}{p} \quad (2-25)$$

$$m_{v,0} = \frac{x_{v,0}}{1-x_{v,0}} \frac{m_a M_{H_2O}}{M_a} \quad (2-26)$$

Next, assuming that air is a non-participating medium in terms of radiation heat transfer, a balance of energy applied to CV3 states that,

$$\dot{Q}_{23} - \dot{Q}_{34} - \dot{Q}_{3\infty} + \dot{m}_{v,in} h_g(T_2) - \dot{m}_{v,out} h_g(T_3) = \frac{dU_v}{dt} + \frac{dU_a}{dt} \quad (2-27)$$

Where,

$$\dot{Q}_{23} = U_{23} A_{23} (T_2 - T_3) \quad (2-28)$$

$$\dot{Q}_{3\infty} = U_{3\infty} A_{3\infty} (T_3 - T_\infty) \quad (2-29)$$

$$\dot{Q}_{34} = U_{34} A_{34} (T_3 - T_4) \quad (2-30)$$

$$\frac{dU_i}{dt} = m_i c_i \frac{dT_i}{dt} \quad (2-31)$$

$c_i$  = specific heat at constant volume for substance "i"

$$\frac{dU_v}{dt} + \frac{dU_a}{dt} = (m_a c_a + m_v c) \frac{dT_3}{dt} \quad (2-32)$$

Therefore,

$$\begin{aligned} & U_{23} A_{23} (T_2 - T_3) - U_{34} A_{34} (T_3 - T_4) - U_{3\infty} A_{3\infty} (T_3 - T_\infty) \\ & + \dot{m}_{v,in} h_g(T_2) - \dot{m}_{v,out} h_g(T_3) = (m_a c_a + m_v c) \frac{dT_3}{dt} \end{aligned} \quad (2-33)$$

### 2.3.2 Mass and energy analysis of CV4 (roof of cogeneration system):

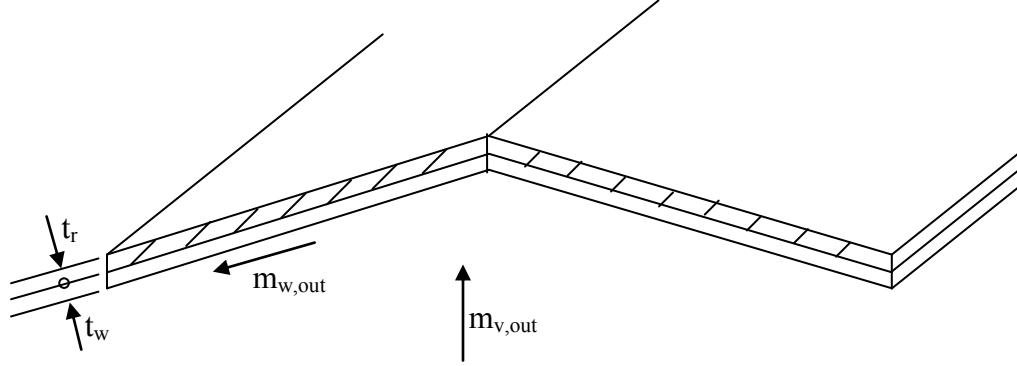


Figure 2.3: Control volume 4 (roof of cogeneration system).

CV4 consists of the roof and the thin layer of condensed water ( $t_w$ ) that forms in time. Assuming  $t_r$  as a design parameter and  $t_w \approx 1$  mm as a model fixed parameter, which effect on the results is to be investigated numerically and experimentally,

Mass conservation applied to CV4 states that:

$$\frac{dm_{w,4}}{dt} = \dot{m}_{v,out} - \dot{m}_{w,out} \quad (2-34)$$

It should be noted that  $m_{w,4} = 0$ , when  $t=0$ , and  $m_{w,max} = \rho_w V_{4,w}$ ,  $V_4 = V_{4,r} + V_{4,w}$ .

Therefore,  $\dot{m}_{w,out} = 0$ , until  $m_w = m_{w,max}$ , then  $\dot{m}_{w,out} = \dot{m}_{v,out}$ .

Thus, it is possible to know the time when the condensed water will start to flow through the channels.

A balance of energy applied to CV4 states that:

$$\dot{Q}_{34} - \dot{Q}_{4\infty} + \dot{m}_{v,out} h_g(T_3) - \dot{m}_{w,out} h_f(T_4) = \frac{dU_r}{dt} + \frac{dU_{w,4}}{dt} \quad (2-35)$$

Where  $T_4 = T_\infty$ , where  $t=0$ .

$$\dot{Q}_{34} = U_{34} A_{34} (T_3 - T_4) \quad (2-36)$$

$$\dot{Q}_{4\infty} = U_{4\infty} A_{4\infty} (T_4 - T_\infty) \quad (2-37)$$

$$\frac{dU_r}{dt} + \frac{dU_{w,4}}{dt} = (m_r c_r + m_{w,4} c) \frac{dT_4}{dt} \quad (2-38)$$

Therefore,

$$\begin{aligned}
 & U_{34}A_{34}(T_3 - T_4) - U_{4\infty}A_{4\infty}(T_4 - T_\infty) + \dot{m}_{v,out}h_g(T_3) - \dot{m}_{w,out}h_f(T_4) \\
 & = (m_r c_r + m_{w,4}c) \frac{dT_4}{dt} \quad (2-39)
 \end{aligned}$$

### 2.3.3 Mass and energy analysis of CV2 (water in cogeneration system):

A balance of energy applied to CV2 states that:

$$-\dot{Q}_{23} + \dot{Q}_{12} - \dot{Q}_{2\infty} + \dot{m}_{v,in}(h_f(T_{w,in}) - h_g(T_2)) = \frac{dU_{w,2}}{dt} \quad (2-40)$$

Where,

$$\dot{Q}_{23} = U_{23}A_{23}(T_2 - T_3) \quad (2-41)$$

$$\dot{Q}_{12} = U_{12}A_{12}(T_1 - T_2) \quad (2-42)$$

$$\dot{Q}_{2\infty} = U_{2\infty}A_{2\infty}(T_2 - T_\infty) \quad (2-43)$$

$$\frac{dU_{w,2}}{dt} = m_w c \frac{dT_2}{dt} \quad (2-44)$$

Therefore,

$$\begin{aligned}
 & -U_{23}A_{23}(T_2 - T_3) + U_{12}A_{12}(T_1 - T_2) - U_{2\infty}A_{2\infty}(T_2 - T_\infty) \\
 & + \dot{m}_{v,in}(h_f(T_{w,in}) - h_g(T_2)) = m_w c \frac{dT_2}{dt} \quad (2-45)
 \end{aligned}$$

One assumption considered while analyzing CV2 is that the water is fed into CV2 from an outside source at a temperature which is equal to the temperature  $T_2$  of CV2 and at the same rate at which it is evaporated out of CV2.

### 2.3.4 Energy analysis of CV1 (photovoltaic cell):

$$\dot{Q}_{rad} - \dot{Q}_{1\infty} - \dot{Q}_{12} - P = \frac{dU_{PV}}{dt} \quad (2-46)$$

Where,

$$\dot{Q}_{rad} = [\alpha_{PV}\dot{I} - \varepsilon_{PV}\sigma(T_1^4 - T_\infty^4)]A_{12} \quad (2-47)$$

$$\dot{Q}_{1\infty} = U_{1\infty}A_{1\infty}(T_1 - T_\infty) \quad (2-48)$$

$$\dot{Q}_{12} = U_{12}A_{12}(T_1 - T_2) \quad (2-49)$$

$P$ - Power generated by the PV cell, given in (2-11)

$$\frac{dU_{PV}}{dt} = m_{PV}c_{PV} \frac{dT_1}{dt} \quad (2-59)$$

Therefore,

$$[\alpha_{PV}\dot{I} - \varepsilon_{PV}\sigma(T_1^4 - T_\infty^4)]A_{12} - U_{1\infty}A_{1\infty}(T_1 - T_\infty) - U_{12}A_{12}(T_1 - T_2) - P = m_{PV}c_{PV} \frac{dT_1}{dt} \quad (2-60)$$

The analysis of CV1 to CV4 delivers the evaporated and produced condensed water in time,  $\dot{m}_{w,out}$ , and the temperature of CV1 to CV4. From the temperatures of different control volumes, it is possible to evaluate:

- i) The electrical power (electrical energy) produced by the PV cell as follows,

$$\dot{E}_{PV} = \dot{W}_{PV} = VI \quad (2-61)$$

Where,

$$I = i(V, T_1, \dot{I}) \quad (2-62)$$

$V$  is the voltage, which is selected by power tracking device to achieve maximum power from the PV system.

- (ii) The total energy required to evaporate the water is considered in calculation of efficiency of the cogeneration system; it is the product of the mass rate of water multiplied by the latent heat of evaporation.

$$\dot{E}_w = \dot{m}_{w,out}(LH_{evap.}) \quad (2-63)$$

Where,

$LH_{evap.}$  is the latent heat of evaporation of water.

The first law efficiency for the system is computed as,

$$\eta_I = \frac{\dot{m}_{w,out} LH_{evap.} + \dot{W}_{PV}}{\dot{I}A_{PV}} \quad (2-64)$$

The increase in efficiency of the system is discussed in the results.

## CHAPTER 3

### METHODOLOGY AND MATERIALS

For the proposed implementation of the PV cell into a cogeneration system, two experiments were required to be carried out, one to simulate the thermal behavior of the cell and the other to simulate the I-V characteristic of the PV cell.

#### **3.1 Experiment to characterize I-V curves of Solara SM 200 S.**

The first experiment was carried out to help us model the I-V characteristic of the PV cell. A photovoltaic cell ‘Solara SM 200 S’ consisting of 36 modules in series was placed on a surface along with pyranometer in such a manner so that the face of the PV cell was parallel to the pyranometer. The pyranometer used for the experiment was ‘Apogee PYR-PA5’, an amplified pyranometer which gave an output in volts. The connections of the pyranometer are shown in the schematic below. To measure the irradiance incident on the PV cell, care was taken to place the measuring face of the pyranometer exactly parallel to the PV cell; since the pyranometer read different irradiances at different incident angles. The surface on which the PV cell was placed in our case was a wooden plank. It was taken care that there is good ventilation between the back of the PV cell and the wooden surface so that air trapped behind the PV cell did not get heated up and increase the PV cell temperature and thus provide spurious results.

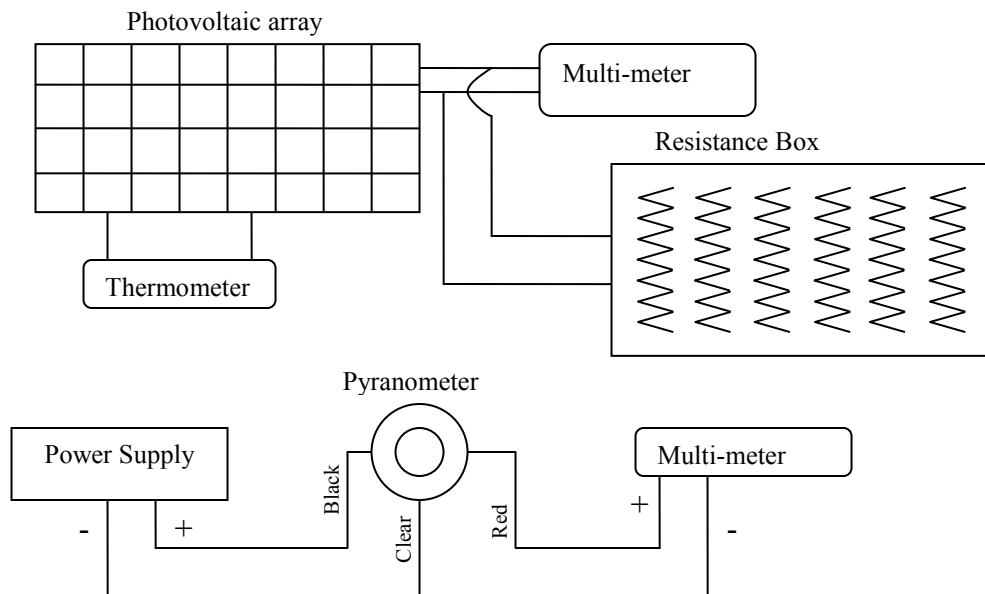


Figure 3.1: Schematic of I-V characteristic measurements.

A connection was set up to measure the irradiance independently using a 5V DC power supply which gave power to the amplified pyranometer which in turn produced a voltage which was proportional to the irradiance incident on its measuring face. This voltage was measured by a multi-meter. The conversion factor for this voltage to irradiance was  $0.25 \text{ W/m}^2$  per mV. The multi-meter used to measure the voltage is a Fluke, true-rms Multi-meter 87/EIII. Figure 3.2 shows the arrangement of the pyranometer.

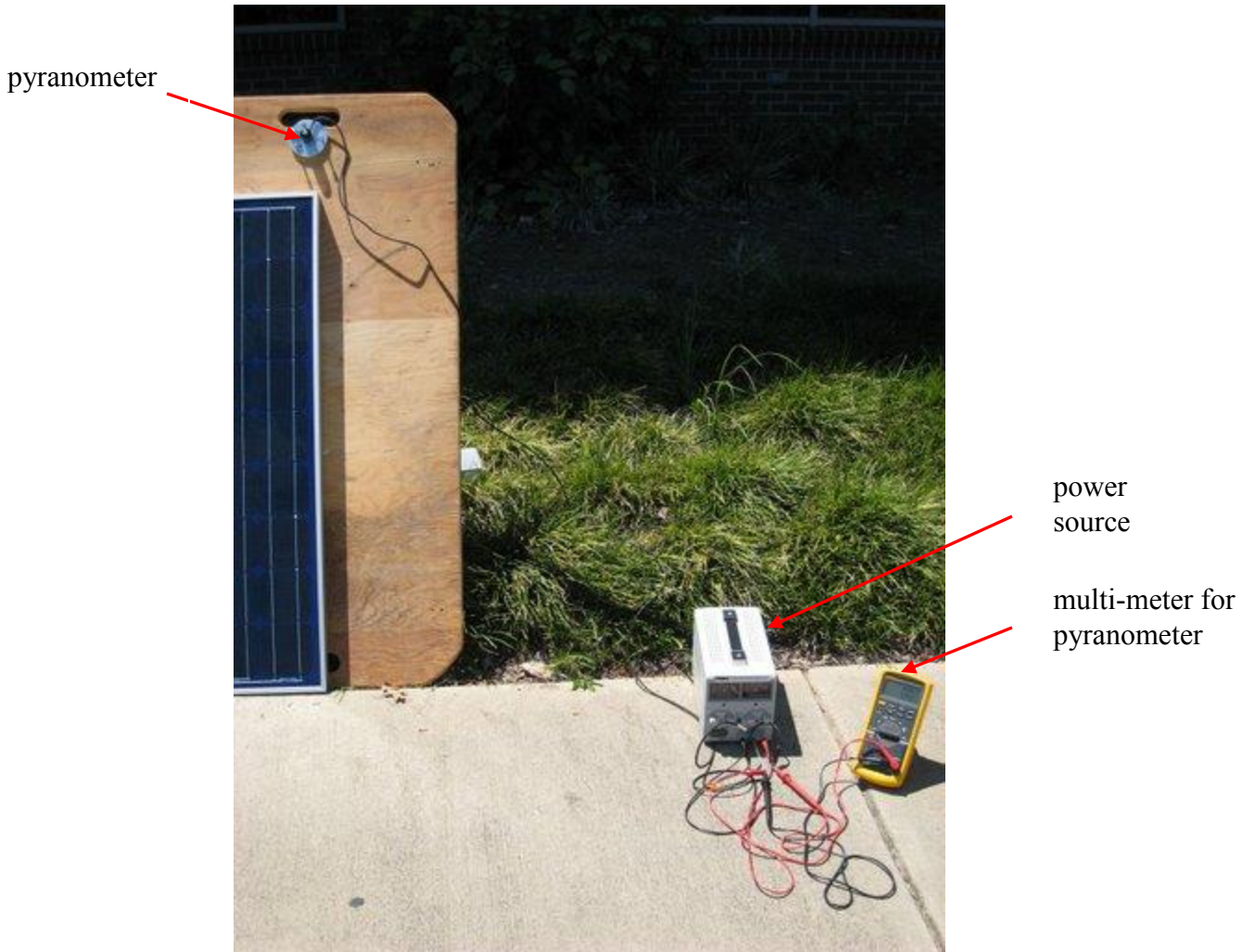


Figure 3.2: Arrangement of the pyranometer.

To measure the temperature, we used two Omega surface mount K type thermocouples CO1; we ensured proper thermal contact by applying OmegaTherm 201, a high thermally conducting paste to the thermocouples and fixing it to the PV cell by insulation tapes. These thermocouples were attached at the back side of the PV cell, although, to measure the exact temperature of the PV junction requires constructional changes, a close model is provided in [3] where the temperature of the junction is estimated as

$$T_c = T_m + \Delta T \left( \frac{E}{E_o} \right) \quad (3.1)$$

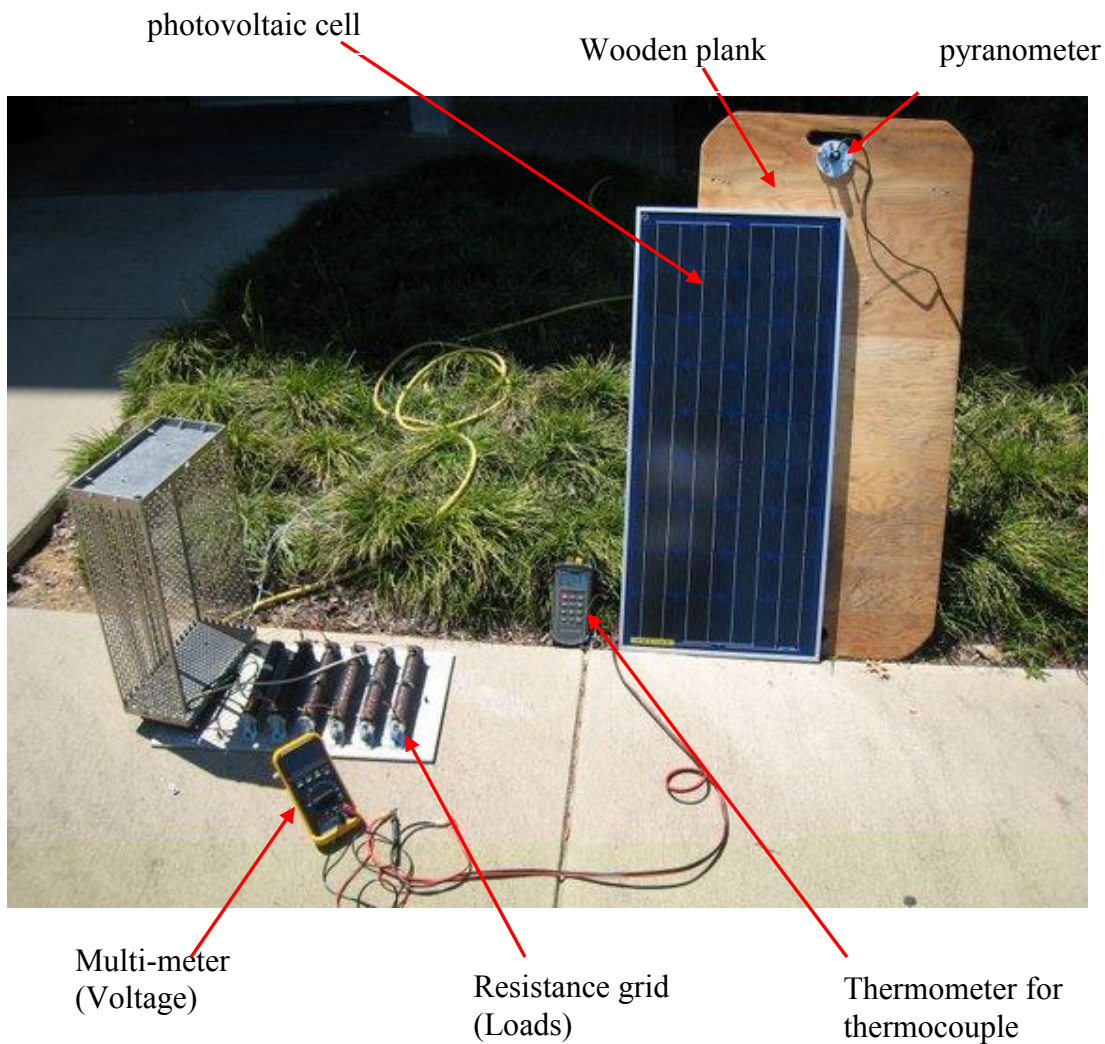


Figure 3.3: Arrangement to measure the current voltage characteristics of photovoltaic cell.

Where  $T_m$  is the temperature at the back of the cell and  $E_o$  is the irradiance  $1000\text{W/m}^2$  and  $\Delta T$  is  $3^\circ\text{C}$  for Tedlar surface. The temperature was measured directly by plugging the connectors on the other end into the Extech J/K type thermometer (#421502). The thermometer gives the temperature in Celsius as well as in Fahrenheit.

As shown in the schematic, the connections from a multi-meter are clamped to the ends of the connections from the PV cell. These connections from the PV cell along with the clamps from the multi-meter are connected to the resistances to measure the output voltage from these resistances. The multi-meter used to measure the voltage is a Fluke, True-rms Multi-meter 87/EIII. The arrangement is shown in Figure 3.3.

The PV system was exposed to sunlight. The irradiance is noted from the Pyranometer. The temperature of the PV system was noted by the thermometer. The open circuit voltage  $V_{OC}$  and the short circuit current  $I_{SC}$  is measured by the multi-meter. A series of measurement of voltages at different resistances from the resistance box is carried out. This reading of voltages at different resistances generates the I-V curve of the PV system at the given temperature and irradiance. It was seen that the temperature and the irradiance during the measurements of voltages was constant while measuring the voltages at each resistance, this would generate voltages which would represent the I-V curve at a given temperature and irradiance. Thus different measurements of I-V were taken by varying the temperature and irradiance independently.

The irradiance was varied by adjusting the surface on which the PV cell was resting to the desired angle. By adjusting the angle of incidence of the sun on to the PV cell surface, the irradiance could be varied. The irradiance measured on a sunny day with blue sky with the sunrays normal to the surface of the PV cell was roughly  $1000 \text{ W/m}^2$ . Thus different measurements were taken at different irradiances by changing the angle of incidence of the sunrays. The same effect of changed irradiance is seen when there is a cloud cover on the PV cell, but the cloud cover is not constant for the time taken to measure the voltages over the resistance box. Hence, to get the measurements at constant irradiance, they were taken by varying the irradiance by varying the angle of incidence of the sunrays.

The temperature can be varied to high temperature and low temperature. Achieving low temperature was difficult if trying to cool the PV system by artificial methods. Low temperature was achieved by a more natural way by performing the experiment on a cold day with temperature of  $30^\circ\text{F}$ . Even when the ambient temperature is  $30^\circ\text{F}$ , because of the irradiance incident on the PV surface, the temperature of the PV surface goes on increasing; a low temperature was achieved by providing forced convection to the PV surface with the help of a high velocity air circulator. The lowest temperature at which the experiment was performed was  $15^\circ\text{C}$ . A high temperature was achieved by performing the experiment on a hot day with temperature of around  $80^\circ\text{F}$ ; the PV cell surface temperature was increased and went up to  $130^\circ\text{F}$ .

### 3.2 Experiment to verify the thermal model of the photovoltaic system

The ‘Solara SM 200 S’, a photovoltaic cell consisting of 36 modules in series was used to verify the thermal model of the photovoltaic system. The photovoltaic cell was connected to a pre-decided value of resistance to complete the circuit. The resistance value was chosen such that the power produced by the PV cell would be  $\pm 20\%$  of the peak power value. This peak power for a given irradiance and temperature was calculated from the double exponential model of the PV cell. A thermometer measured the voltage coming out of the PV cells. An amplified pyranometer, ‘Apogee PYR-PA5’ was used to measure the irradiance; the connections were set in the same manner as in the experiment described above to measure the voltage. The voltage measured is then converted to irradiance by a factor  $0.25 \text{ W/m}^2$  per mV.

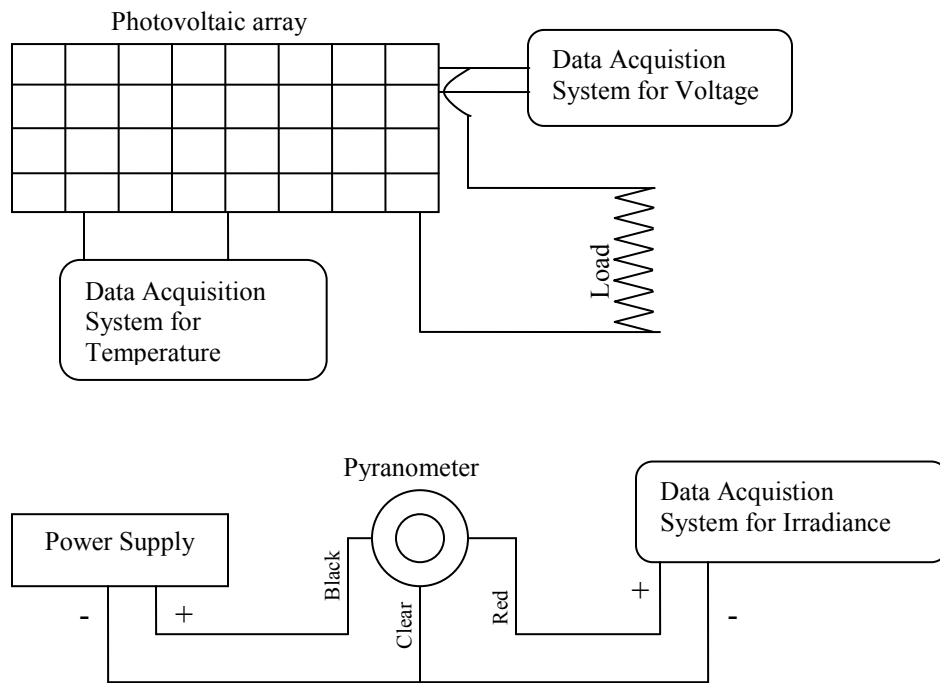


Figure 3.4: Measurement of unsteady state Temperature of PV cell.

Two Omega surface mount K type thermocouples CO1 were used to measure the temperature; we ensured proper thermal contact by applying OmegaTherm 201, a high thermally conducting paste to the thermocouples and fixing it to the PV cell by insulation

tapes. These thermocouples were attached at the back side of the PV cell as explained in the earlier experiment. The temperature was measured by connecting a thermometer system to these two thermocouples to measure the voltage, which gives temperature of the PV cell. Thus the temperature, irradiance and voltage are measured simultaneously for a given time interval. This data is used to verify the model of the PV cell. The arrangement of the thermocouples is shown in Figure 3.5.

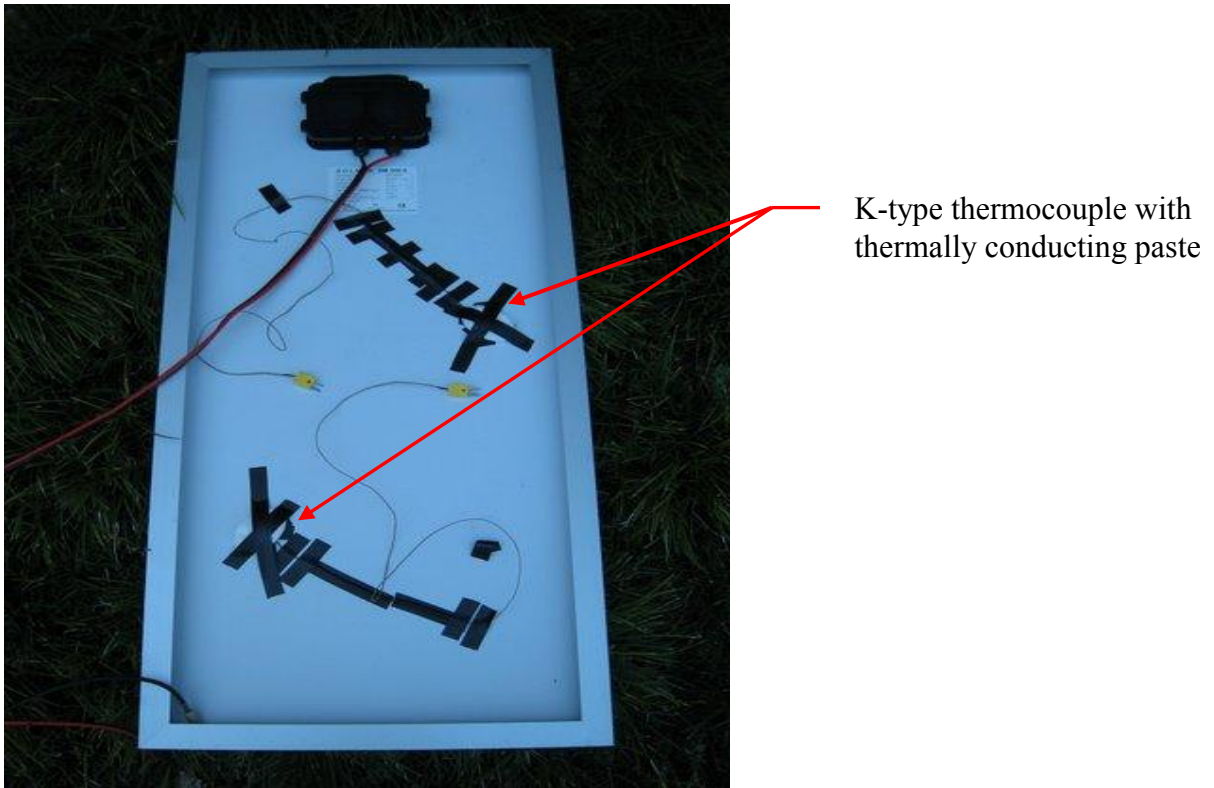


Figure 3.5: Back of photovoltaic cell with thermocouples stuck with high thermally conducting paste.

The data obtained from this experiment is used to prepare a thermal model of the PV cell and compare its temperature which is measured by the thermometer.

## CHAPTER 4

### RESULTS AND DISCUSSION

#### 4.1 Photovoltaic cell performance.

This chapter describes our implementation of the numerical solution to the problem modeled in the previous chapter.

The I-V equation of the photovoltaic cell is given by

$$I = I_{ph} - I_{s1} \left( e^{\frac{e_0 \cdot V}{m_1 \cdot k \cdot T}} - 1 \right) - I_{s2} \left( e^{\frac{e_0 \cdot V}{m_2 \cdot k \cdot T}} - 1 \right) - \frac{(V + IR_s)}{R_p} \quad (4-1)$$

The equation shown above has 5 parameters which are dependent on temperature and irradiance. For a Silicon photovoltaic cell, these 5 parameters are dependent on temperature and irradiance in a manner which are given by the equations from [11]

$$I_{ph} = K_0 E (1 + K_1 T) \quad (4-2)$$

$$I_{s1} = K_2 T^3 e^{\left(\frac{K_3}{T}\right)} \quad (4-3)$$

$$I_{s2} = K_4 T^{\left(\frac{3}{2}\right)} e^{\left(\frac{K_5}{T}\right)} \quad (4-4)$$

$$R_s = K_6 + \frac{K_7}{E} + K_8 T \quad (4-5)$$

$$R_p = K_9 e^{(K_{10} T)} \quad (4-6)$$

There are 11 constants ( $K_0$  to  $K_{10}$ ) which are unique to a given photovoltaic cell. Experiments were done on a Solara SM 200 S at different conditions of temperature (T) and irradiance (E), to characterize the I-V curves; the result for a particular temperature and irradiance were curve-fitted to find the 5 parameters of the double exponential equation, one set of results for a particular temperature and irradiance generated one set of these 5 parameters. Different sets of parameters were obtained from different conditions of temperature and irradiance. These sets were solved simultaneously and averaged to find out the 11 constants of the above equations. They were found to be

$K_0 = 3.3329e-3$	$K_1 = -2.3e-4$	$K_2 = 760.329$	$K_3 = -13965.5$
$K_4 = 10.112$	$K_5 = -6572.85$	$K_6 = -0.11202$	$K_7 = 9.99809$
$K_8 = 3.77e-4$	$K_9 = 9726.41$	$K_{10} = -0.01309$	

Now that we have these 11 constants, the 5 parameters of the double exponential equation of the photovoltaic cell were calculated from the equations (4-2) to (4-6) for any set of temperature and irradiances. Using these parameters, a Newton-Raphson solution was used to calculate the current for the given voltages from the double exponential equation and thus generate the I-V curve for the photovoltaic cell for a set of temperature and irradiance. The comparison of some of the results which are calculated with the experimental values at given irradiance and temperatures for the Solara SM 200 S is shown below.

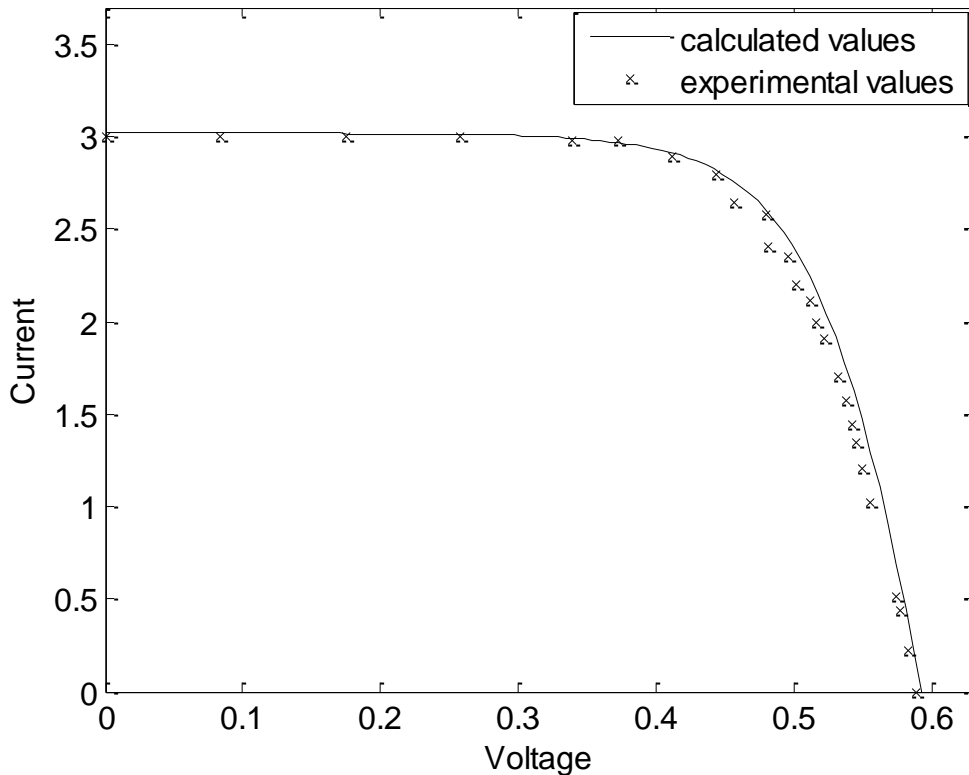


Figure 4.1: Comparison of calculated and experimental values of I-V characteristics for 300K module temperature and irradiance of 975 W/m<sup>2</sup>.

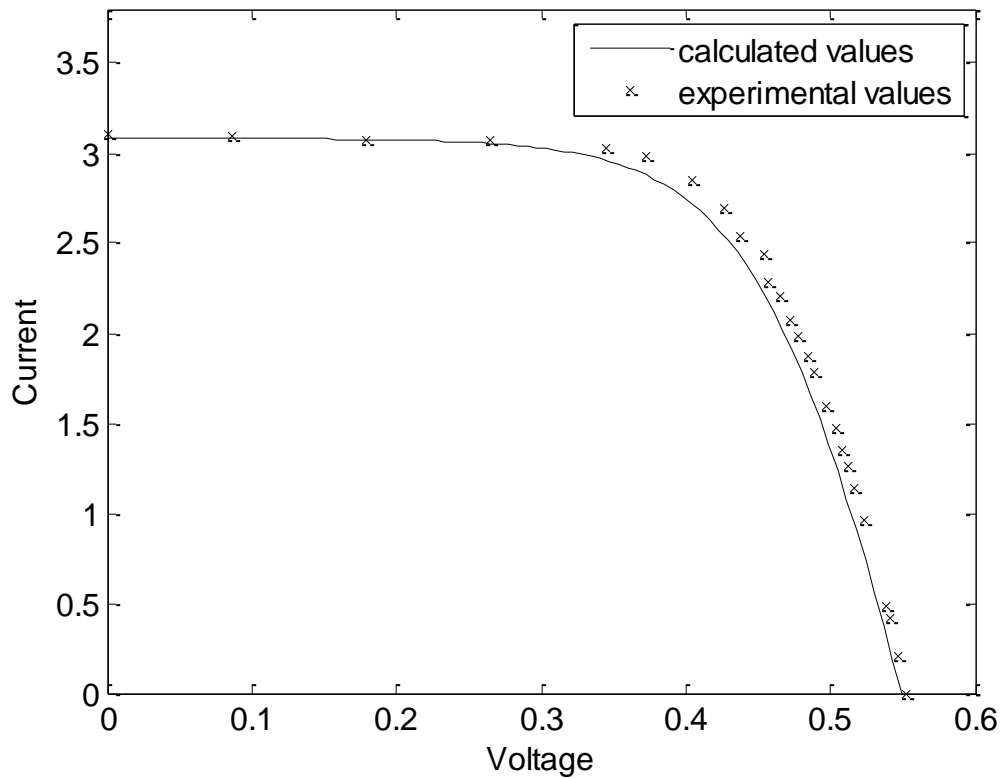


Figure 4.2: Comparison of calculated and experimental values of I-V characteristics for 323K module temperature and irradiance of 1000 W/m<sup>2</sup>.

Figures 4.1 and 4.2 show characteristics of current and voltage. Figure 4.1 shows these characteristics at a higher irradiance of 975 W/m<sup>2</sup>, the current almost reaches the maximum current  $I_{\max}$  of the photovoltaic cell. Figure 4.2 also shows the characteristics at a very similar irradiance of 1000 W/m<sup>2</sup>. It is seen that as the temperature of the module increases, the voltage produced by the cell decreases even as the irradiance on it is increased, thus producing lower power. This is a characteristic of the photovoltaic cell. To increase the efficiency of the photovoltaic cell, it needs to be kept at a low temperature. There are several ways to cool the photovoltaic cell. This report analyzes one way of keeping the temperature of the photovoltaic cell lower than what it would typically reach.

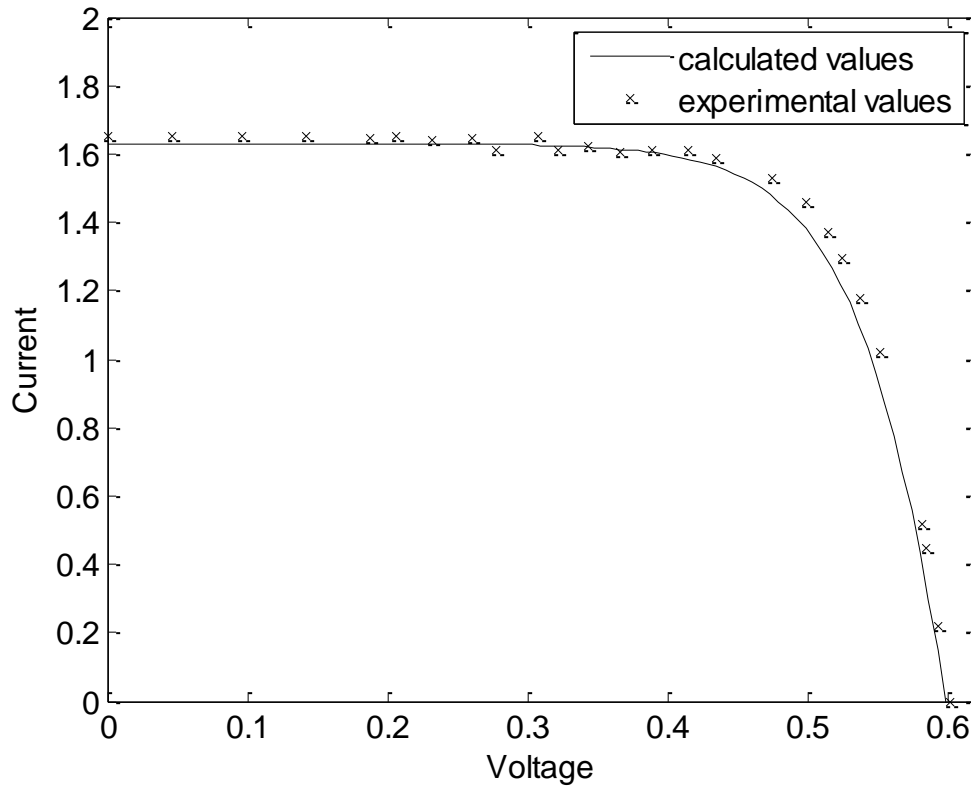


Figure 4.3: Comparison of calculated and experimental values of I-V characteristics for 289K module temperature and irradiance of 525 W/m<sup>2</sup>.

Figure 4.3 shows the current decreases as the irradiance decreases, the current value is directly proportional to the irradiance. The power is directly proportional to the irradiance but it is inversely proportional to the temperature of the module. Any decrease in the module temperature increases the power and thus increasing the efficiency of the photovoltaic cell.

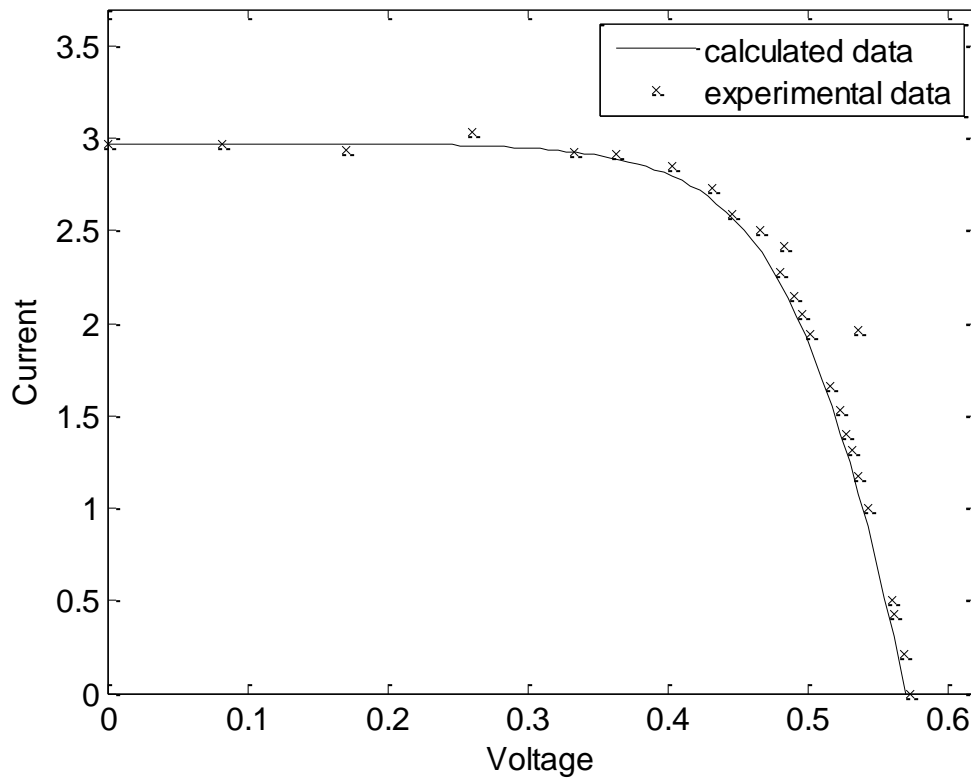


Figure 4.4: Comparison of calculated and experimental values of I-V characteristics for 312K module temperature and irradiance of 962.5 W/m<sup>2</sup>.

Figures 4.1 to 4.4 compare the experimental values and the values of currents for all voltages calculated by solving the double exponential equation for different conditions of irradiance and temperature. From the Figures above, we see that there is an error of less than 8% in the values of currents for the given voltages, between the calculated values and the experimental values. Thus the I-V curve for the cell at any temperature and irradiance can be generated by plugging in these 5 parameters in the double exponential equation. Once the I-V curve is generated, then by using a power tracking device, the maximum power point on this I-V curve can be found, and the voltage at that point is the voltage at which the current needs to be extracted in order to have maximum efficiency of the photovoltaic cell.

Thus this model of the photovoltaic cell is incorporated in the co-generation system to find out the exergy taken out of the available irradiation from Control Volume 1 of the co-generation system.

## 4.2 Thermal model of photovoltaic cell

The thermal model of the photovoltaic cell is given by the equation,

$$\left[ \alpha_{PV} \dot{I} - \varepsilon_{PV} \sigma (T_1^4 - T_\infty^4) \right] A_{12} - U_{1\infty} A_{1\infty} (T_1 - T_\infty) - P = m_{PV} c_{PV} \frac{dT_1}{dt} \quad (4-7)$$

which is an initial value problem. It consists of a first order non linear differential equation; the solution of the differential equation explains how the photovoltaic cell reaches steady state with respect to time. The initial temperature of the cell is taken at ambient at 298K. The cell reaches a constant temperature at constant irradiation. The behavior of the cell with constant irradiance is shown in Figure 4.5. The graph is plotted at irradiance of  $1000 \text{ W/m}^2$ . The global coefficient of heat transfer is taken as  $3.75 \text{ W/m}^2\text{K}$ . The value of the global coefficient is validated with experimental observation.

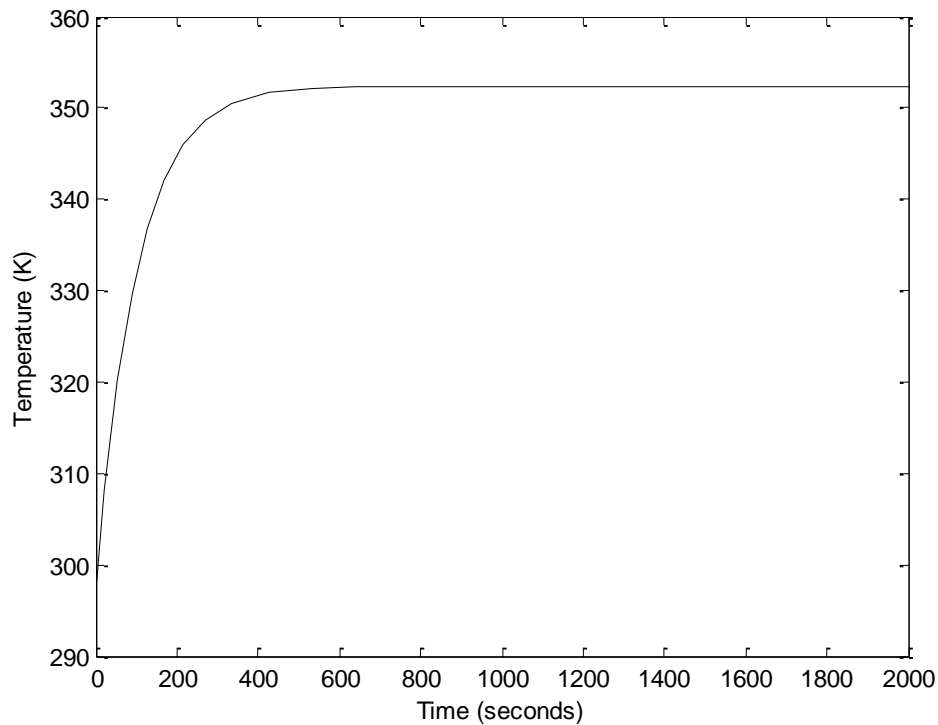


Figure 4.5: Variation of the temperature of photovoltaic module with respect to temperature for a given constant irradiation ( $1000 \text{ W/m}^2$ ).

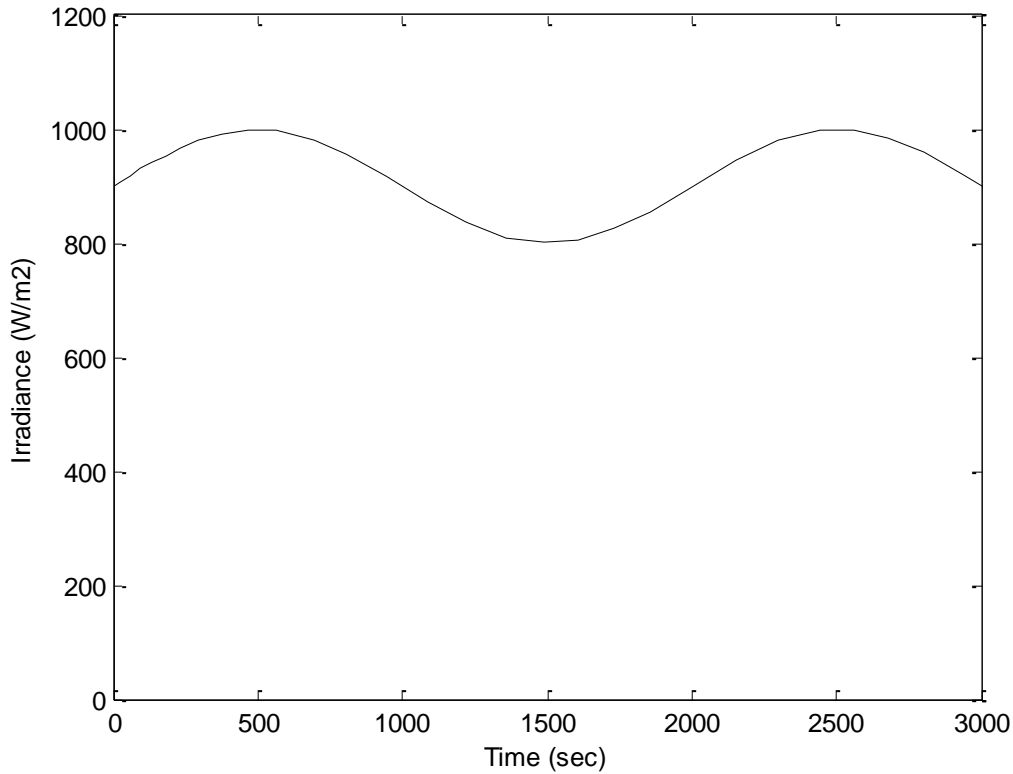


Figure 4.6: Irradiation varying in a sinusoidal manner with respect to time.

Figure 4.6 shows a varying irradiance with time. This varying irradiance is used to show the behavior of the cell module with respect to varying temperature. The Figure 4.7 shows the graph of temperature of the module with a sinusoidal varying irradiation with the global coefficient of heat transfer taken as  $3.75 \text{ W/m}^2\text{K}$ . We experience constant irradiation only on rare occasions. The irradiance constantly keeps changing with changing cloud conditions. This model predicts the temperature of the module in conditions of varying irradiance fairly. In the Figure 4.6 it is seen that the temperature rises from ambient temperature and decreases as the irradiance decreases and increases as the irradiance increases. This is the general behavior of the cell as the heat received by the cell increases as the irradiance increases and decreases as the irradiance decreases.

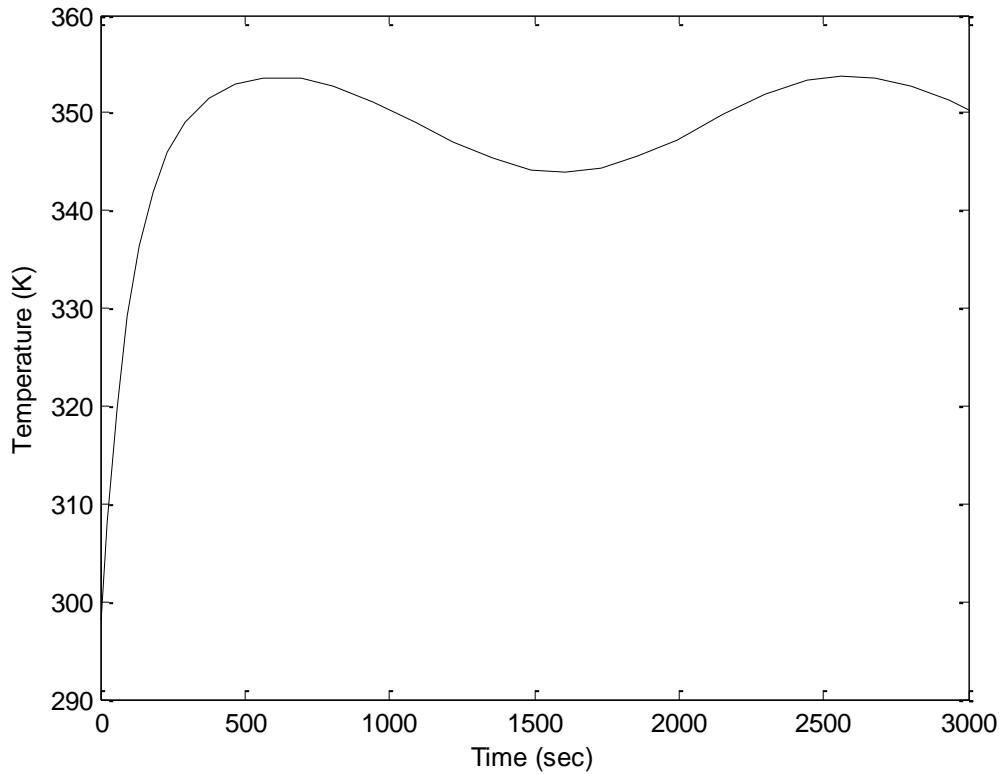


Figure 4.7: Plot of temperature of module with varying irradiance.

### 4.3 Thermal model of cogeneration system

This section describes our implementation of the numerical solution to the problem modeled in the previous chapter.

The model that is described in the chapter 2 gives rise to a set of equations. The equations (2-13), (2-33), (2-34), (2-39), (2-45) and (2-60) together form an initial value problem. This constitutes a system of first order, non linear, ordinary differential equations, the solution to which, explains the behavior of the system by giving us the variation of the mass of vapor, the mass rate of distilled water in the respective control volumes, the variation of temperatures of the respective control volumes with respect to time.

The equations (2-13), (2-33), (2-34), (2-39), (2-45) and (2-60) can be shuffled and rewritten as shown below,

$$\frac{dm_v}{dt} = \dot{m}_{v,in} - \dot{m}_{v,out} \quad (4-8)$$

$$\frac{dm_{w,4}}{dt} = \dot{m}_{v,out} - \dot{m}_{w,out} \quad (4-9)$$

$$\frac{dT_1}{dt} = \frac{[\alpha_{PV}\dot{I} - \varepsilon_{PV}\sigma(T_1^4 - T_\infty^4)]A_{12} - U_{1\infty}A_{1\infty}(T_1 - T_\infty) - U_{12}A_{12}(T_1 - T_2) - P}{m_{PV}c_{PV}} \quad (4-10)$$

$$\frac{dT_2}{dt} = \frac{[-U_{23}A_{23}(T_2 - T_3) + U_{12}A_{12}(T_1 - T_2) - U_{2\infty}A_{2\infty}(T_2 - T_\infty) + \dot{m}_{v,in}(h_f(T_{w,in}) - h_g(T_2))]}{m_w c} \quad (4-11)$$

$$\frac{dT_3}{dt} = \frac{[U_{23}A_{23}(T_2 - T_3) - U_{34}A_{34}(T_3 - T_4) - U_{3\infty}A_{3\infty}(T_3 - T_\infty) + \dot{m}_{v,in}h_g(T_2) - \dot{m}_{v,out}h_g(T_3)]}{(m_a c_a + m_v c)} \quad (4-12)$$

$$\frac{dT_4}{dt} = \frac{U_{34}A_{34}(T_3 - T_4) - U_{4\infty}A_{4\infty}(T_4 - T_\infty) + \dot{m}_{v,out}h_g(T_3) - \dot{m}_{w,out}h_f(T_4)}{(m_r c_r + m_{w,4}c)} \quad (4-13)$$

Table 4.1: Values of some parameters and constants considered during the simulation.

Parameter	Value	Comments	
$U_{23}, U_{34}, U_{2\infty},$ $U_{3\infty}, U_{4\infty}$	$10 \frac{W}{m^2 K}$	Global heat transfer coefficient, a lumped heat transfer coefficient considering applicable modes of heat transfer.	
$U_{1\infty}$	$3.75 \frac{W}{m^2 K}$	Global heat transfer coefficient between the CV1 and atmosphere.	
$U_{12}$	Varying as explained below.	Global heat transfer coefficient between the CV1 and CV2, lumped heat transfer coefficient considering natural convection and conduction.	
$\frac{g \cdot \beta}{\alpha \cdot \nu_a}$	$90.7e6 \frac{1}{m^3 K}$	for dry air @ 30°C	
$\alpha$	$0.223e-4 \frac{m^2}{s}$	for dry air @ 30°C	
$\nu_a$	$0.16e-4 \frac{m^2}{s}$	for dry air @ 30°C	
Sc	0.6	Schmidt number for water vapor	
D	D (m <sup>2</sup> /s)	T <sub>3</sub> (K)	Mass diffusivity of air-water vapor gases at T <sub>3</sub>
	2.6e-5	298	
	2.88e-5	313	
$\alpha_{PV}$	0.855	Absorptivity of photovoltaic cell [13]	
$\epsilon_{PV}$	0.85	Emissivity of photovoltaic cell [13]	
$c_{PV}$	$2.918 \frac{KJ}{kg K}$	Specific heat of photovoltaic cell	

The numerical solution to the system of ordinary differential equations given by equations (4-8) to (4-13) was implemented in MATLAB using the Runge-Kutta method. The accuracy in simulation was set to a value 0.0001. The integration time was set so

that it was sufficient to reach the steady state. The initial state conditions were specified as

$$\begin{aligned} T_1 &= T_{\text{amb}} & T_2 &= T_{\text{amb}} \\ T_3 &= T_{\text{amb}} & T_4 &= T_{\text{amb}} \\ m_v &= 0 & m_{w,4} &= 0 \end{aligned}$$

One assumption made while analyzing CV2 is that the mass of vapor evaporated from CV2 is replenished with water at temperature of CV2, such that the volume of water in CV2 always remains constant.

The mass flow rate  $m_v$  in CV3 was analyzed as

$$\frac{dm_v}{dt} = \dot{m}_{v,in} - \dot{m}_{v,out}$$

Where  $\dot{m}_{v,in}$  is mass of vapor coming into CV3 from CV2 by evaporation and was found by the mass transfer coefficient. The condition for mass going out of CV3 is taken as

$$\begin{aligned} \dot{m}_{v,out} &= 0 \text{ if (relative humidity of CV3), } \phi < 1, \\ &= \dot{m}_{v,in} \text{ if } \phi = 1. \end{aligned}$$

The assumption taken in the above expression is that when the relative humidity in CV3 is less than 1, vapor keeps accumulating in CV3. When relative humidity of CV3 is equal to one, then the vapor produced is going out of CV3 into CV4 and starts condensing on the surface. Another assumption made is that a thin uniform layer of water forms on the roof surface before water starts dripping out of CV4 which is taken as  $\dot{m}_{w,out}$  in the analysis below. The thickness of this layer ( $t_r$ ) is a design parameter and is taken as 1mm. This condition is taken into the analysis as follows

$$\frac{dm_{w,4}}{dt} = \dot{m}_{v,out} - \dot{m}_{w,out}$$

Where  $m_{w,4}$  is the mass of water in CV4 and  $\dot{m}_{v,out}$  is the mass of vapor coming out of CV3 and coming into CV4. The condition for mass going out of CV4 is taken as

$$\begin{aligned} \dot{m}_{w,out} &= 0 \text{ if } m_{w,4} < m_{w,4, \text{max}} \\ &= \dot{m}_{v,out} \text{ when } m_{w,4} = m_{w,4, \text{max}} \end{aligned}$$

which says that there is no water coming out of CV4 until the mass of water in CV4 reaches its maximum which equals  $m_{w,4,max} = \rho_w V_{4,w}$ , where  $V_{4,w}$  is the volume of water in the layer of thickness ( $t_r$ ) formed on the roof surface.

First we plot the behavior of different control volumes with respect to time for a constant irradiation. Later we study the behavior of the different control volumes with respect to time for irregular irradiance. The irradiance is plotted by a sinusoidal curve with amplitude of  $100 \text{ W/m}^2$  and the period of 2000 seconds. The figures below illustrate the evolution of different parameters with time to reach the steady state for constant irradiation.

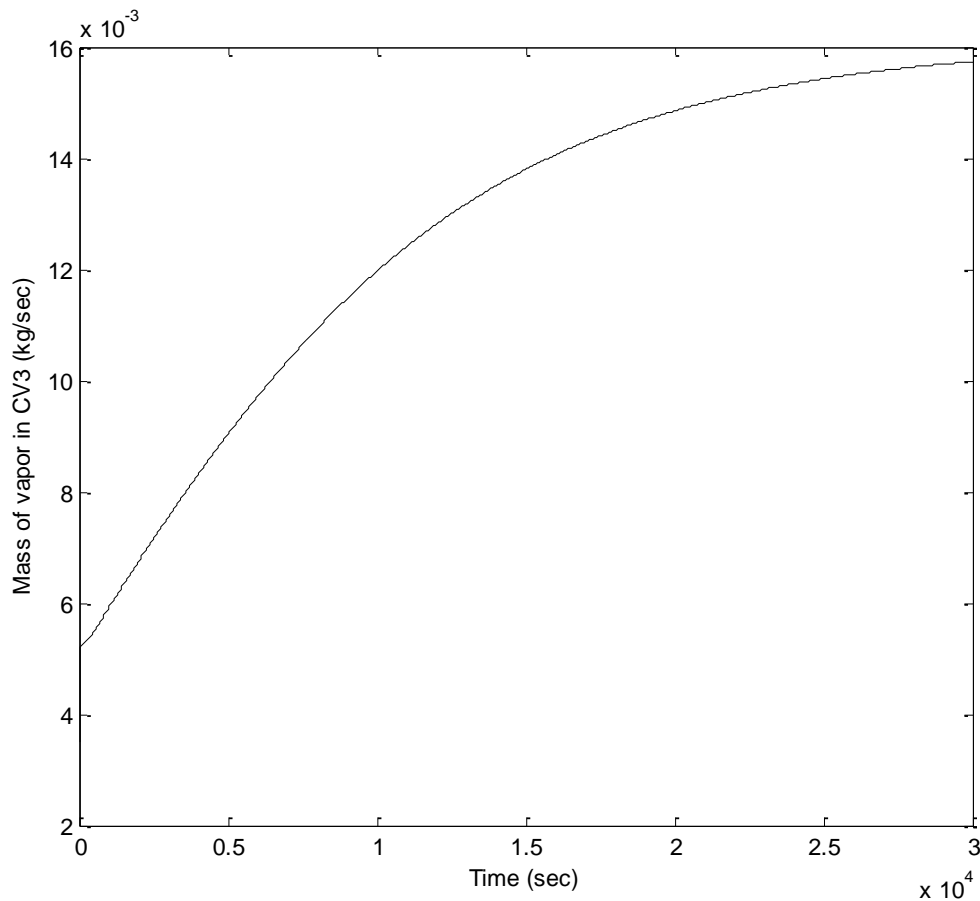


Figure 4.8: Variation of mass of vapor ( $m_v$ ) with time.

The Figure 4.8 shows the variation of mass of vapor in CV3, at initial state the mass of vapor in CV3 depends on the relative humidity of air, as time progresses the mass of vapor in CV3 increases, in sometime the relative humidity in CV3 approaches 1, at this point the vapor starts to condense on the roof surface, from this point onwards since relative humidity is 1, the mass of vapor in CV3 should appear to be constant, but it keeps on increasing as the temperature of CV3 increases, the amount of vapor that is accommodated in CV3 increases even though the relative humidity in CV3 is 1. The mass of vapor in CV3 goes on increasing till the temperature of CV3 reaches steady state, from this point on the mass of vapor in CV3 remains constant. The irradiance in this case was kept constant at  $1000 \text{ W/m}^2$ .

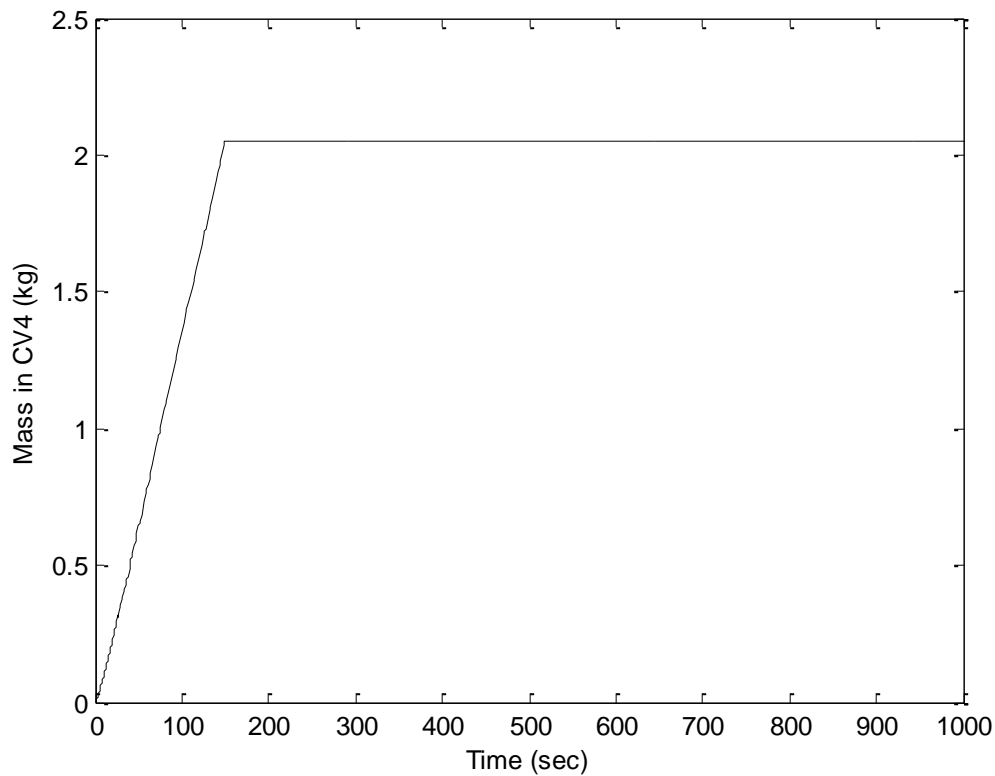


Figure 4.9: Variation of mass of water in CV4 with time.

The Figure 4.9 shows the variation of the mass of water that is condensing on the surface of the roof (CV4). The mass of water in the roof increases from zero to a value 2.052 kg, which is a design parameter with is set as per the thickness of the water film which is

assumed to be 1mm in thickness. After the mass of water reaches this value, it starts flowing out of the CV4, thus the mass of water in CV4 remains constant which is shown in the figure above. The irradiance in this case was kept constant at  $1000 \text{ W/m}^2$ .

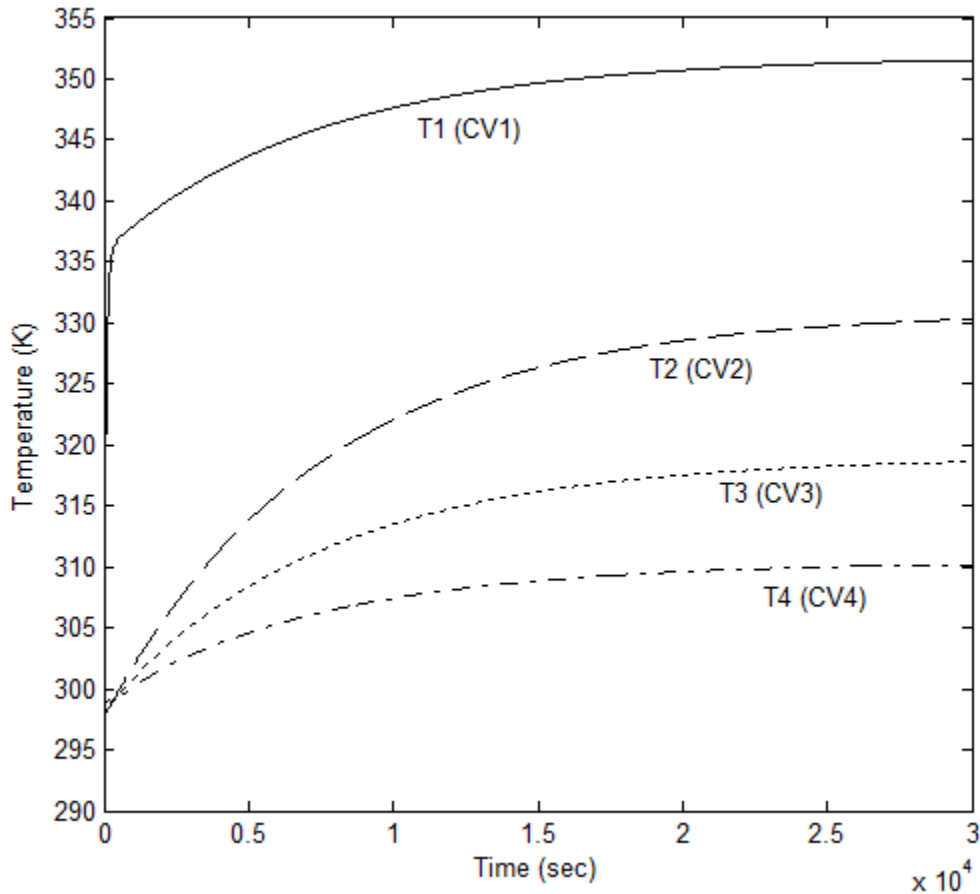


Figure 4.10: Temperature variation of different control volumes with time.

Figure 4.10 shows the variation of temperature of different control volumes with respect to time. The initial condition of all the control volumes was set to ambient temperature. As time progresses, eventually all the control volumes reach steady state constant temperature.

As shown in the figure, the temperature of photovoltaic cell (CV1) increases until it reaches a steady state, for the assumed irradiation and atmospheric conditions. At  $1000 \text{ W/m}^2$  irradiation and given atmospheric conditions and a given set of values of the global

heat transfer coefficient, the cell temperature reaches almost 352 K. The effect of the variation of these heat transfer coefficients is discussed later.

For the water body in the enclosure (CV2), the initial water temperature is assumed as ambient temperature, which increases until it reaches steady state; the level of water in CV2 is maintained constant and is replenished with outside water at temperature of CV2. This is one of the assumptions made in calculations, thus the condition of mixing of different temperatures is avoided.

The initial temperature of the vapor space (CV3) is also assumed at ambient temperature and it increases until it reaches a steady state. The relative humidity approaches 1 with time, since the temperature of CV3 increases with time, the mass of vapor in CV3 also increases until the temperature of CV3 reaches a steady state.

The temperature of roof of enclosure (CV4) also increases until it reaches a steady state. CV4 is emitting heat to the surrounding with a large area; hence the temperature of CV4 is lowest compared to other control volumes. The temperature of CV4 reaches steady state as time increases.

A model for the temperature of a bare PV module was made as explained above; this model was validated by the experimental observations that were made. The temperature achieved was compared to the temperature attained when the photovoltaic cell is placed in the cogeneration system. The global heat transfer coefficients  $U_{12}$  was varied from 10  $W/m^2K$  to 1000  $W/m^2K$  and the varying temperatures were plotted. The figure of the varying temperature for different coefficients is shown in Figure 4.11.

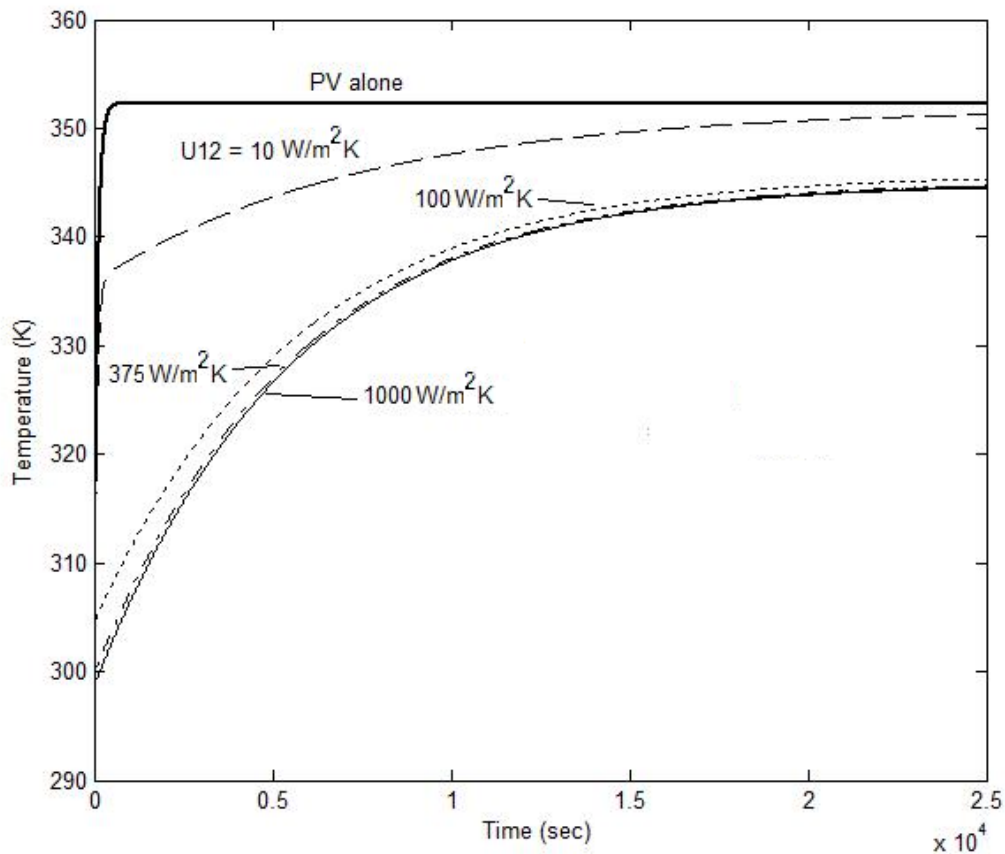


Figure 4.11: Graph of temperature vs. time for different values of global heat transfer coefficient ( $U_{12}$ ).

From the Figure 4.11 it can be seen that as the value of global heat transfer coefficient increases, the heat transfer increases, the temperature of CV1 decreases as the heat transfer rate increases. But after a certain value of the global heat transfer coefficient, any increase in the coefficient does not effect to lower the temperature of CV1, as it almost attains the value of CV2, as the heat transfer is very effective. The behavior of the photovoltaic cell is such that a lower temperature produces a higher efficiency.

Hence with the global heat transfer coefficient  $U_{12}$  as 100 W/m<sup>2</sup>K the temperatures of the control volumes vary as shown in the Figure 4.12 below.

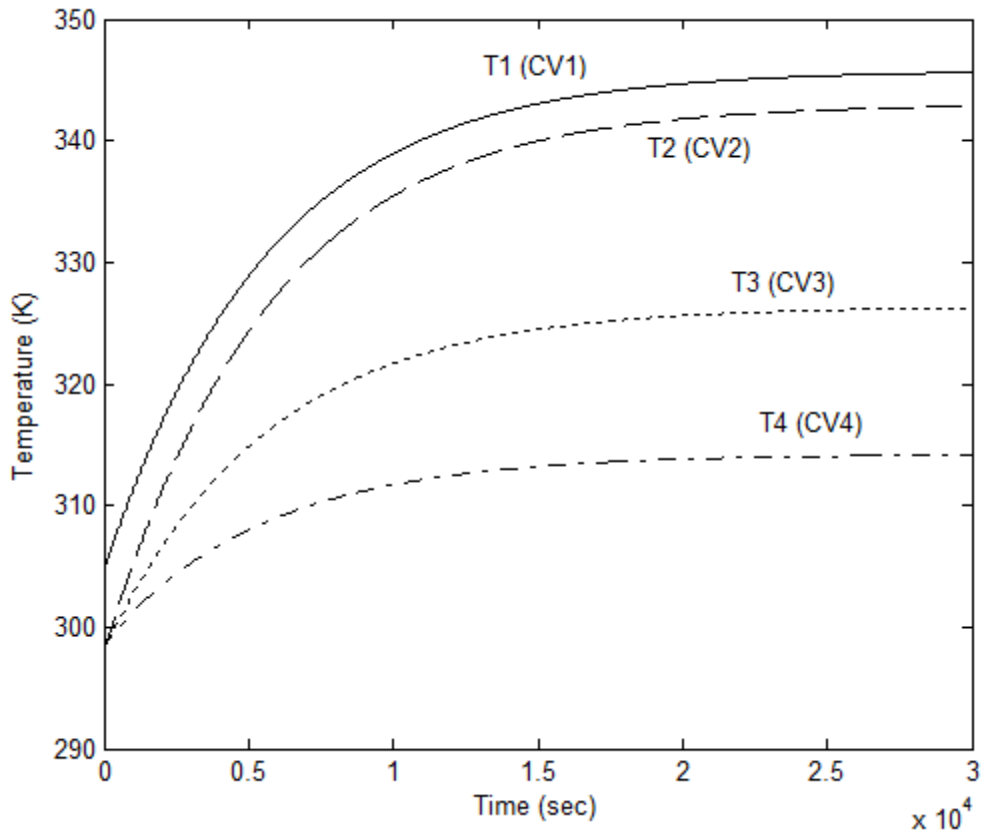


Figure 4.12: Temperature variation of different control volumes with time ( $U_{12}=100$   $W/m^2K$ ).

From Figure 4.12 it can be seen that as the heat transfer between CV1 and CV2 increases, the temperature of CV1 reduces and the temperature of CV2 increases, due to this increase in the CV2 temperature, there is more evaporation of water in the CV3 and the mass of vapor in CV3 and thus the quantity of distilled water out of CV4 increases. The variation of vapor in CV3 for the value of  $U_{12} = 100$  is shown in Figure 4.13.

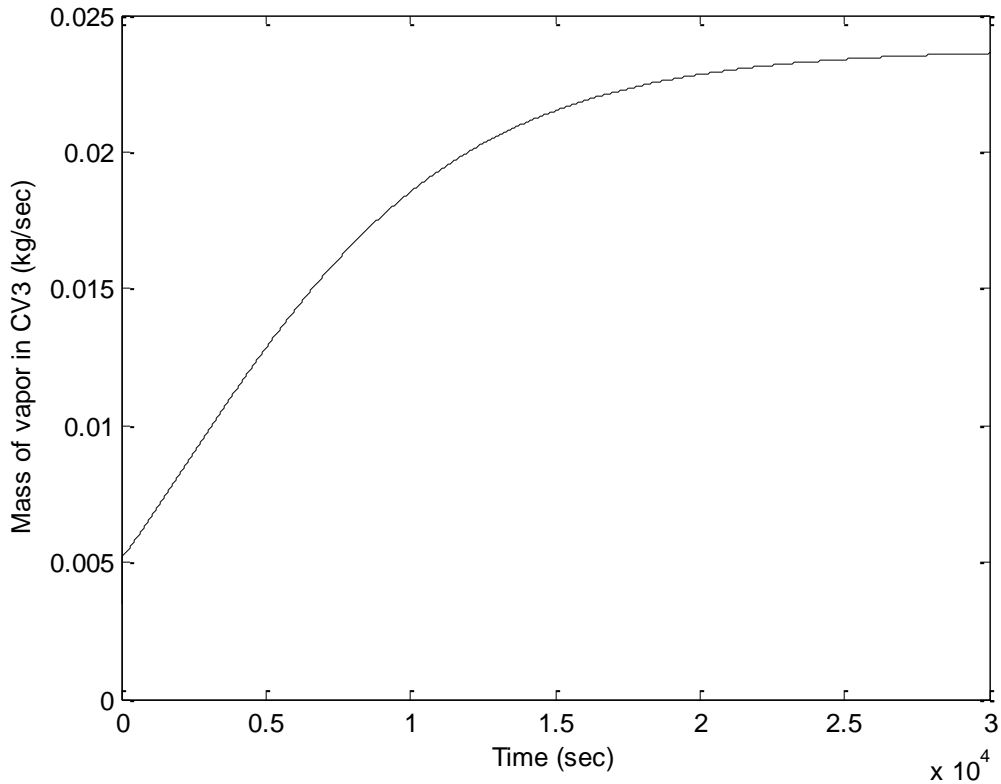


Figure 4.13: Variation of mass of vapor with time ( $U_{12} = 100\text{W/m}^2\text{K}$ ).

Thus with increased amount of vapor in the CV3, the exergy related to the vapor also increases. At steady state the vapor produced is the rate at which distilled water is produced in CV4. Thus higher heat transfer results in the increase in the production of water and the reduction of temperature of CV1. The reduction of temperature of CV1 also increases the exergy of photovoltaic cell as shown below.

The cogeneration system causes the temperature of the PV cell to be 345.8 K as compared to the PV alone to be 352.3 K. The IV characteristics of the PV cell at both the temperatures at a given irradiation was plotted, which are shown in Figure 4.14. The plot of power verses voltage is shown in Figure 4.15; the graph has a higher peak at lower temperature which shows that the efficiency of the PV cell with the cogeneration system is higher.

The IV characteristics and the power characteristics of Solara SM200S at the two temperatures and atmospheric conditions are shown in the Figure 4.14.

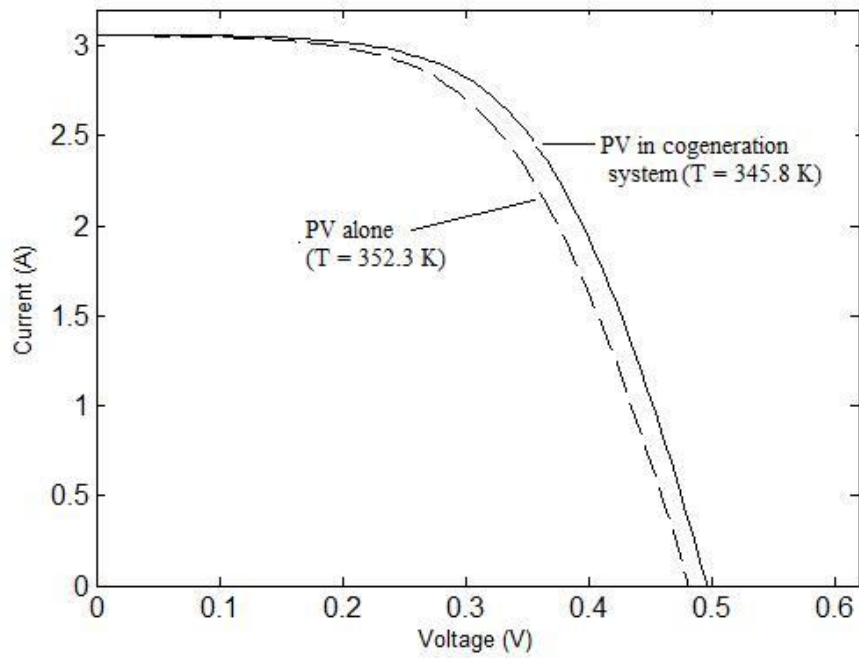


Figure 4.14: Current-Voltage characteristics of photovoltaic cell independently and when coupled with the cogeneration system.

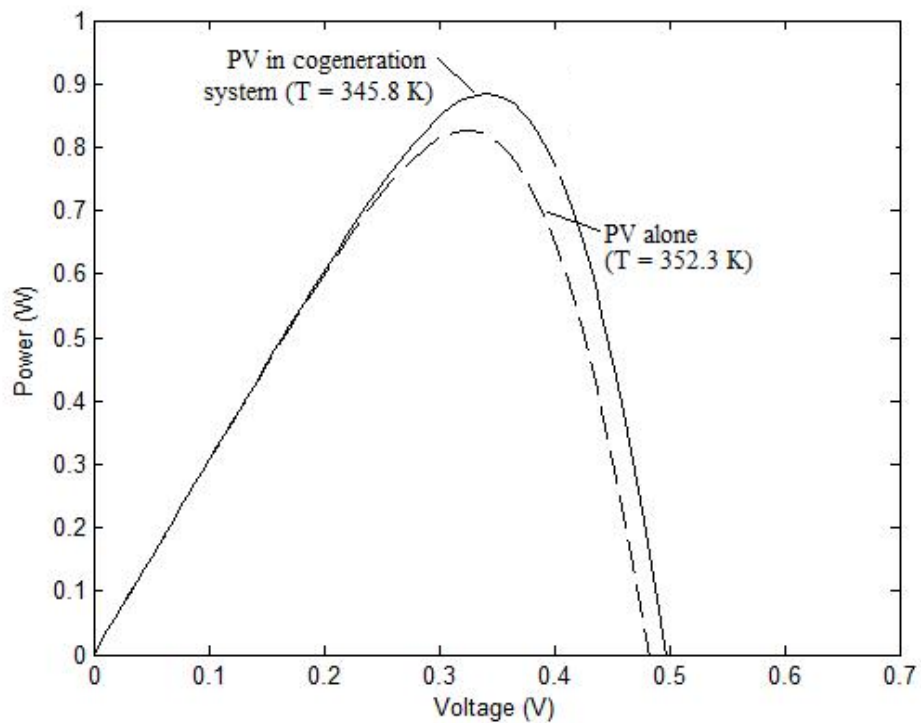


Figure 4.15: Power produced by photovoltaic cell independently and when coupled with cogeneration system.

Figure 4.15 shows that there is an increase in roughly 8% of increase in the peak power by the decrease of temperature from 352.3K to 345.8K. Thus a higher rate of heat transfer not only increases the amount of vapor but also increases the efficiency of the photovoltaic module.

The conditions of the cogeneration system discussed above were taken for a constant irradiation of  $1000 \text{ W/m}^2\text{K}$ . Now we discuss the behavior of the cogeneration system for an irregular irradiation.

The irradiation was changed as per a sine equation, such that the irradiation followed a sine function. The Figure 4.6 shows the variation of irradiance with time. The behavior of the cogeneration system with such a varying irradiance was also plotted and Figure 4.16 shows the variation of temperatures of different control volumes with respect to time. The model gives a fair behavior of the system with the varying irradiance, the temperatures decrease as the irradiance decreases and increase with increasing irradiance.

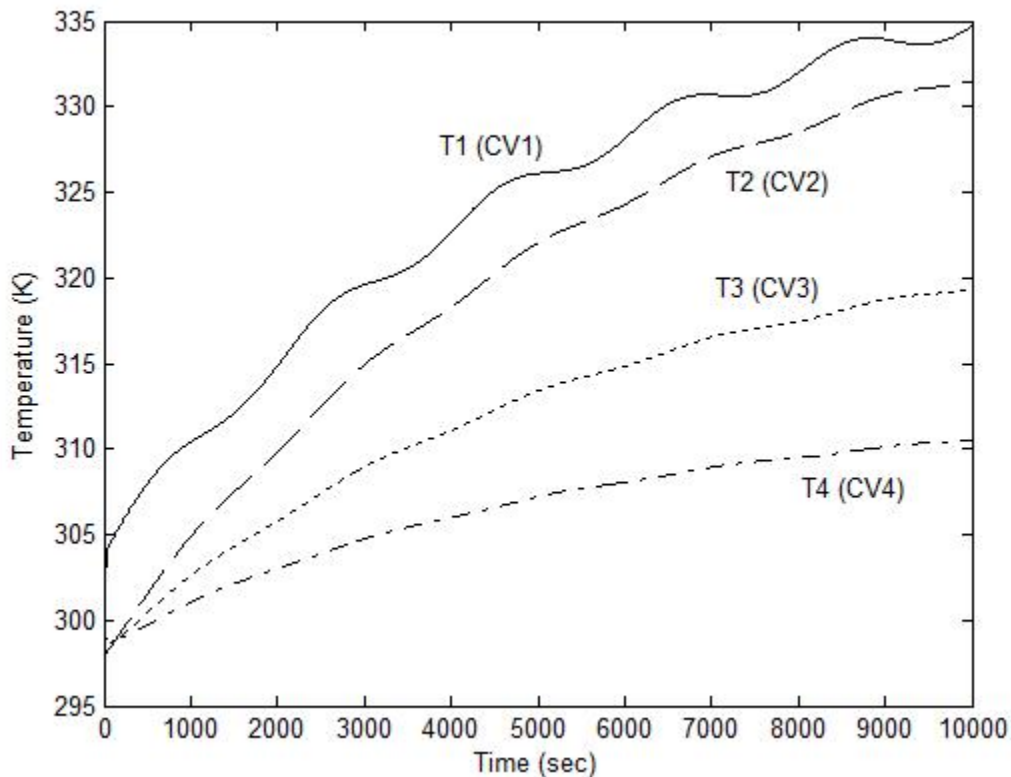


Figure 4.16: Temperature of control volumes under varying irradiance.

The mass of vapor in the vapor space (CV3) also varies with varying irradiance. This variation is shown in Figure 4.17. The variation of mass of vapor in the vapor space is evident, since fewer vapors are produced while the irradiance is low, and the vapors produced increase when the irradiance is high.

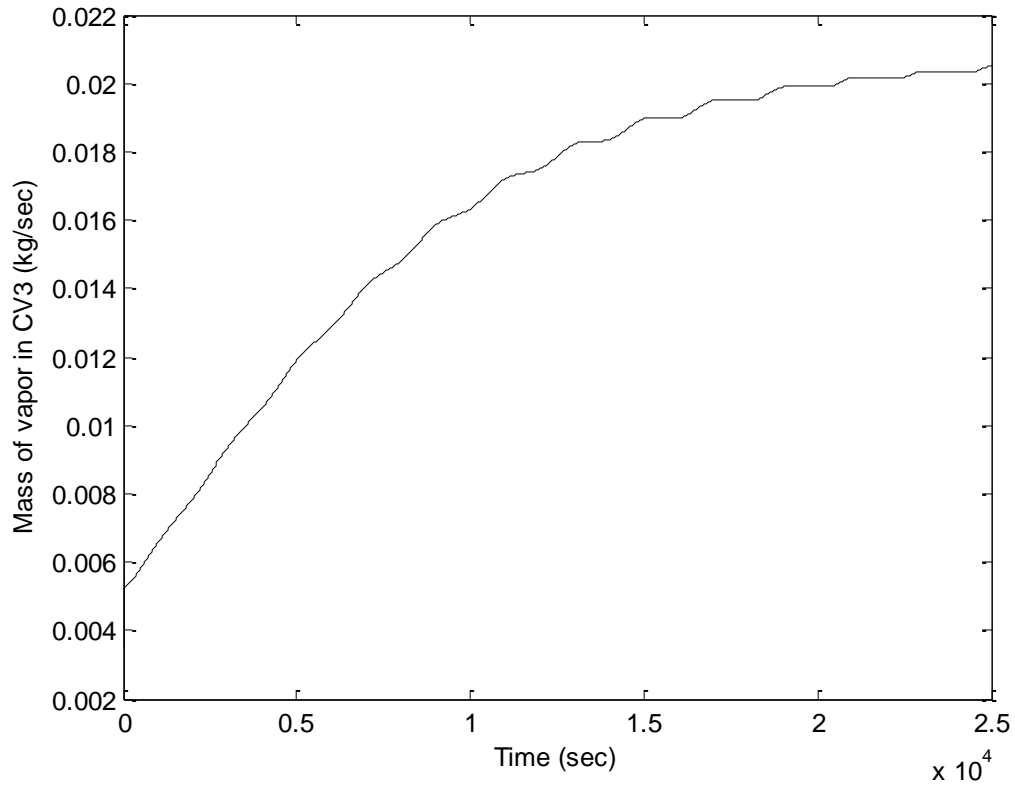


Figure 4.17: Variation of mass of vapor in vapor space (CV3) with time under a varying irradiance.

## CHAPTER 5

### CONCLUSIONS AND SUGGESTIONS

A theoretical model of a cogeneration system is developed to produce fresh water and electricity. The efficiency of the photovoltaic array which generates electricity is increased in the process when combined with the distillation system. This chapter summarizes the some findings of the temperature profiles of different control volumes of the cogeneration system, the water produced in the process, the increase of efficiency of the photovoltaic array and the increase in exergetic efficiency of the system.

The temperature profiles of different control volumes is plotted in Figure 5.1.

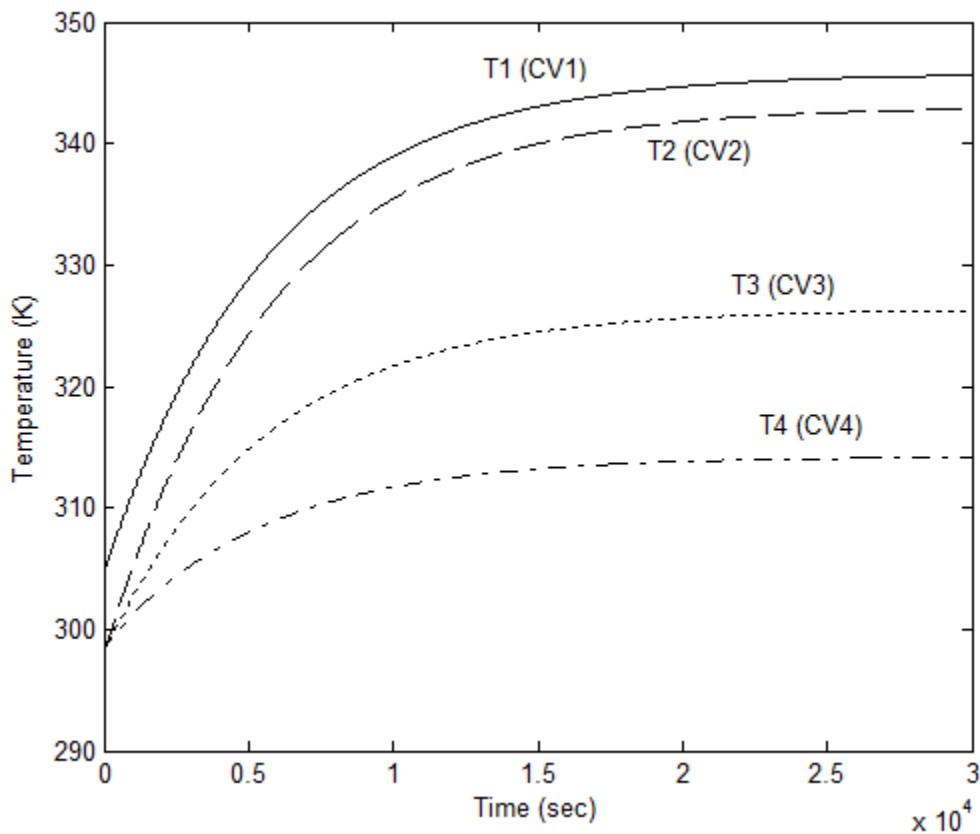


Figure 5.1: Variation of temperature of different control volumes at irradiation of  $1000\text{W/m}^2$  and  $U_{12}$  at  $100\text{ W/m}^2\text{K}$ .

Figure 5.1 shows variation of temperature of different control volumes with time. Under steady irradiation, all the control volumes reach steady state in time. Coupled with the distillation system, on condition with high heat transfer coefficient  $U_{12}$ , the temperature of the photovoltaic cell (CV1) reaches a lower value. The maximum power obtained at this lower temperature is higher than the maximum power obtained if the photovoltaic cell is operating alone. The comparison of temperature of the photovoltaic module coupled with the cogeneration system and the module acting alone is shown in Figure 5.2. This is one case when the irradiation is constant at  $1000 \text{ W/m}^2$ .

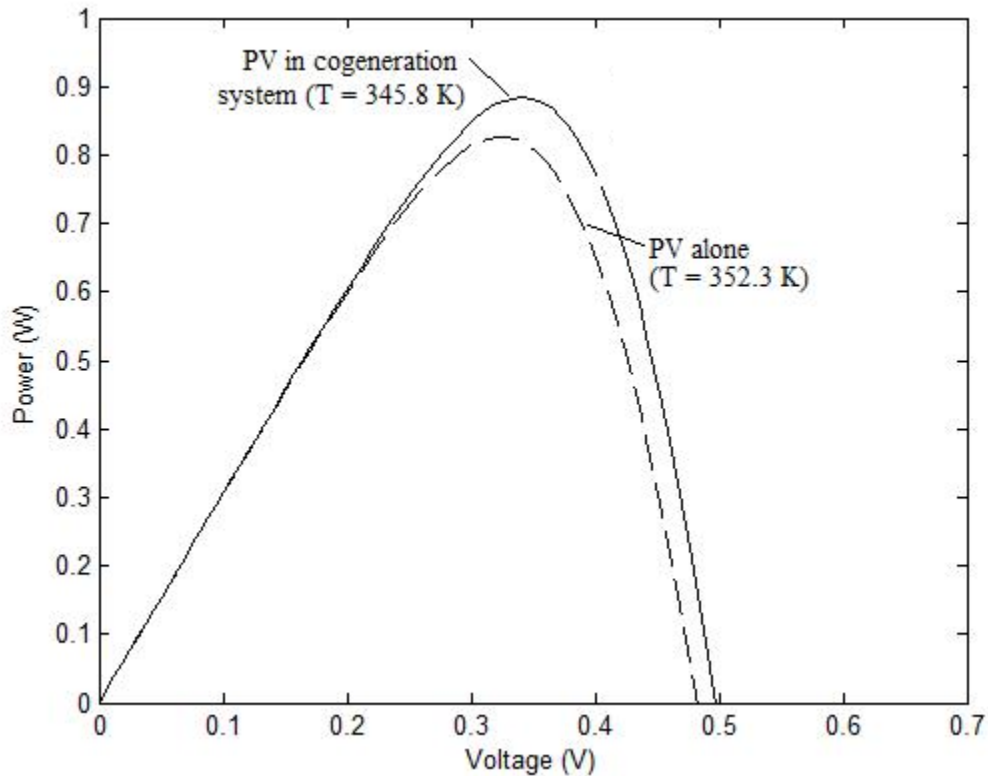


Figure 5.2: Comparison of the power obtained by photovoltaic module.

In this case at  $1000 \text{ W/m}^2$ , the photovoltaic module reaches a temperature of  $345.8\text{K}$  when coupled with the distillation system. The maximum power generated by the photovoltaic cell at  $345.8\text{K}$  is  $\sim 0.9\text{W}$ , compared to the power generated at  $352.3\text{K}$  which is  $\sim 0.8\text{W}$ . There is 10% rise in the efficiency of the photovoltaic cell when coupled with

the distillation system. With higher heat transfer rate, the temperature of the photovoltaic cell will decrease further.

The developed model predicts the generation of water as shown in the Figure 5.3. The amount of water distilled from the system can be increased by having improved heat transfer between the control volumes. This model provides us the tool for efficient and independent water and electricity production.

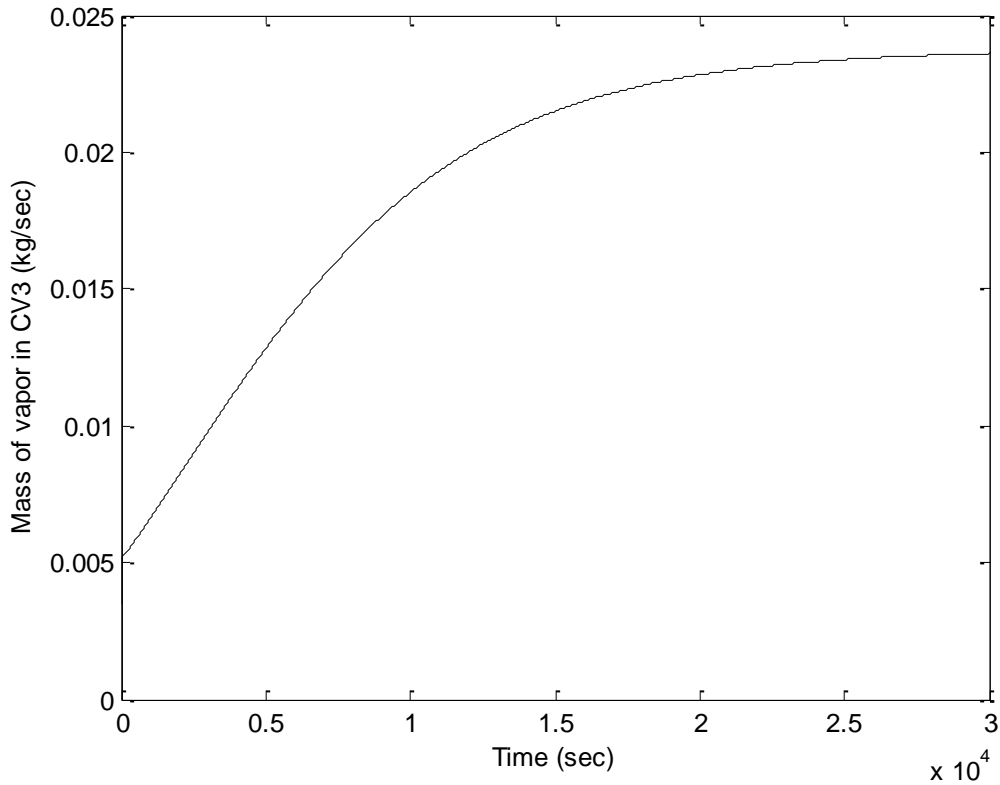


Figure 5.3: Variation of mass of water produced with respect to time.

The results of the cogeneration system are discussed in Chapter 4. The cogeneration system increases efficiency utilizing the heat of solar irradiation along with the solar energy to produce electricity.

As per Equation (2-63), the energy required to vaporize water is given by

$$\dot{E}_w = \dot{m}_{w,out}(LH_{evap.}) \quad (5-1)$$

The vapor produced at  $1000 \text{ W/m}^2$  of irradiation is  $0.024 \text{ kg/sec}$ , thus the energy required to vaporize this amount of vapor is

$$\dot{E}_w = 54.48 \text{ W}$$

The energy produced by a single photovoltaic cell at  $1000 \text{ W/m}^2$  is given in Figure 4.15, is  $0.9 \text{ W}$ . The Solara SM200S has 36 cells in series, hence the total power produced by the cell is  $32.4 \text{ W}$ . The total exergy of the sun which is utilized is the addition on these values which total up to  $86.88 \text{ W}$ .

The exergy which is incident upon the cogeneration system is the given by irradiation incident upon the photovoltaic cell which is  $1000 \text{ W/m}^2$  on the area of the cell. The Solara SM200S has an area  $0.455 \text{ m}^2$ . Hence the energy incident on the system is  $455 \text{ W}$ . Hence the efficiency of the system is

$$\eta_I = \frac{\dot{m}_{w,out} LH_{evap.} + \dot{W}_{PV}}{\dot{I}A_{PV}} \quad (5-2)$$

Thus the efficiency of the system is increased to  $19.1\%$  compared to the  $8\%$  efficiency of the photovoltaic cell alone.

The cogeneration system works as a separate entity and is not dependent on an outside grid or any other consumable sources of energy, but is solely dependent on solar energy which makes this system independent.

Future work on this model is to perform experimentation and improve the lumped heat transfer coefficients. The transitivity of water vapor and the glass surfaces are assumed to be one. Factors involving the opaqueness of the surfaces and the water vapor are to be considered. The model of mixing of water at different temperatures is to be developed in order to incorporate the practical condition of supplying water to the system. Experimentation is to be carried out to model the behavior of the model in unsteady state. A system which places the photovoltaic cell such that the irradiation is normally incident on the cell is to be developed. As the intensity of the solar irradiation changes with the angle of incidence of the cell, it is most advantageous to keep the cell normal to the irradiation at all times.

## REFERENCES

- [1] A. Luque, S. Hegedus. Handbook of Photovoltaic Science and Engineering, John Wiley and sons, 2003.
- [2] F. Lasnier and T. G. Ang. Photovoltaic Engineering Handbook, Taylor & Francis, 1990.
- [3] D. L. King, J. A. Kratochvil, W. E. Boyson. Field experience with a new performance characterization procedure for Photovoltaic arrays. Presented at the 2<sup>nd</sup> world conference and exhibition on photovoltaic solar energy conservation, 1998.
- [4] A. D. Jones and C. P. Underwood. A thermal model for Photovoltaic systems. Solar Energy Vol. 70, No. 4, 2001, pg 349-359.
- [5] M. Mattei, G. Notton, C. Cristofari, M. Muselli, P. Poggi. Calculation of the polycrystalline PV module temperature using a simple method of energy balance. Renewable Energy, Vol. 31, Issue 4, 2006, pg 553-567.
- [6] B. Sandnes, J. Rekstad. A photovoltaic/thermal (PV/T) collector with a polymer absorber plate. Experimental study and analytical model. Applied Thermal Engineering, Vol. 27, Issues 2-3, 2007, pg 275-286.
- [7] V. Quaschnig. Understanding renewable energy systems, Earthscan Publications Ltd., 2005.
- [8] D. Y. Goswami, F. Kreith, J. F. Kreider. Principles of Solar Engineering, Taylor and Francis, 2000.
- [9] M.A. de Blas, J.L. Torres, E. Prieto, A. Garcia. Selecting a suitable model for characterizing photovoltaic devices. Renewable Energy, 25 (2002): pg 371–380.
- [10] (WO/2005/004243) SEMI-CONDUCTOR DEVICES - AN ELBIT SYSTEMS - RAFAEL PARTNERSHIP, K. Philip. Depletion-less photodiode with suppressed dark current and method for producing the same, 2005.
- [11] J. A. Gow, C. D. Manning. Development of a photovoltaic array model for use in power-electronics simulation studies. IEE Proc.-Electr. Power Appl., Vol 146, No. 2, March 1999.
- [12] J. R. Jang, E. Mizutani. Levenberg-Marquardt method for ANFIS Learning.

- [13] G. Notton , C. Cristofari, M. Mattei, P. Poggi, Modelling of a double-glass photovoltaic module using finite differences. Applied thermal engineering, Vol. 25, Issues 17-18, Dec. 2005, pg 2854-2877.
- [14] B. Van der Bruggen, C. Vandecasteele. Distillation vs. membrane filtration: overview of process evolutions in seawater desalination. Desalination. 2002 JUN 10; 143 (3): pg 207-218.
- [15] E. S. Hrayshat, A. E. Al-Rawajfeh. A solar multiple effect distiller for Jordan. Desalination, 220 (2008): pg 558–565.
- [16] F. Banat, R. Jumah and M. Garaibeh. Exploitation of Solar Energy Collected by Solar Stills for Desalination by Membrane Distillation. Renewable Energy, 2002, 25(2), pg 293-305.
- [17] S. A1-Hallaj, M. M. Farid, A. R. Tamimi. Solar desalination with a humidification--dehumidification cycle: performance of the unit, 1998. Desalination, 120 (1998): pg 273-280.
- [18] Multi-stage Flash Distillation (MSF) Desalination process, [www.water-technology.net/projects/shuaiba](http://www.water-technology.net/projects/shuaiba), visited on 09/29/2008.
- [19] A. Bejan. Convection Heat Transfer, 3<sup>rd</sup> Edition, Wiley and sons, 2004.
- [20] Y. A. Cengel. Heat Transfer: A practical approach, 2<sup>nd</sup> Edition, 2002.

## **BIOGRAPHICAL SKETCH**

Nikhil J. Anthony was born in India to Mary and Anthony. He received his Bachelor of Science degree in Mechanical Engineering in June 2001 from the University of Mumbai, India. He worked in mechanical design of process plant equipments for three years before pursuing his Masters degree in Mechanical Engineering at Florida State University. During which he worked under Dr. Juan Ordonez at Center for Advanced Power Systems. Nikhil graduated in the fall of 2008 and decided to work in the construction industry.